



Water Mass Exchanges between the Bay of Bengal and Arabian Sea from Multiyear Sampling with Autonomous Gliders

LUC RAINVILLE,^a CRAIG M. LEE,^a K. ARULANANTHAN,^b S. U. P. JINADASA,^c HARINDRA J. S. FERNANDO,^d W. N. C. PRIYADARSHANI,^b AND HEMANTHA WIJESEKERA^c

^a *Applied Physics Laboratory, University of Washington, Seattle, Washington*

^b *National Aquatic Resources Research and Development Agency, Colombo, Sri Lanka*

^c *Ocean University of Sri Lanka, Colombo, Sri Lanka*

^d *Department of Civil Engineering, Environmental and Earth Sciences, University of Notre Dame, Notre Dame, Indiana*

^e *Naval Research Laboratory, Stennis Space Center, Mississippi*

(Manuscript received 24 November 2021, in final form 26 May 2022)

ABSTRACT: We present high-resolution sustained, persistent observations of the ocean around Sri Lanka from autonomous gliders collected over several years, a region with complex, variable circulation patterns connecting the Bay of Bengal and the Arabian Sea to each other and the rest of the Indian Ocean. The Seaglider surveys resolve seasonal to interannual variability in vertical and horizontal structure, allowing quantification of volume, heat, and freshwater fluxes, as well as the transformations and transports of key water mass classes across sections normal to the east (2014–15) and south (2016–19) coasts of Sri Lanka. The resulting transports point to the importance of both surface and subsurface flows and show that the direct pathway along the Sri Lankan coast plays a significant role in the exchanges of waters between the Arabian Sea and the Bay of Bengal. Significant section-to-section variability highlights the need for sustained, long-term observations to quantify the circulation pathways and dynamics associated with exchange between the Bay of Bengal and Arabian Sea and provides context for interpreting observations collected as “snapshots” of more limited duration.

SIGNIFICANCE STATEMENT: The strong seasonal variations of the wind in the Indian Ocean create large and rapid changes in the ocean’s properties near Sri Lanka. This variable and poorly observed circulation is very important for how temperature and salinity are distributed across the northern Indian Ocean, both at the surface and at depths. Long-term and repeated surveys from autonomous Seagliders allow us to understand how freshwater inflow, atmospheric forcing, and underlying ocean variability act to produce observed contrasts (spatial and seasonal) in upper-ocean structure of the Bay of Bengal and Arabian Sea.

KEYWORDS: Indian Ocean; Monsoons; In situ oceanic observations; Interannual variability; Intraseasonal variability; Seasonal variability

1. Introduction

Upper-ocean processes occurring in the Bay of Bengal have strong impacts on Indian Ocean circulation. Large riverine freshwater (FW) discharge and excess precipitation into the Bay of Bengal produce strongly stratified surface layers, confining the impact of solar warming to relatively shallow mixed layers and thus producing elevated sea surface temperatures (Rao and Sivakumar 2003; Murty et al. 1992). Flow south of Sri Lanka, modulated by the monsoons and

equatorial dynamics, exports FW from the Bay of Bengal, linking the basin with the rest of the Indian Ocean and balancing the large evaporative fluxes of the Arabian Sea (e.g., Schott and McCreary 2001; Vinayachandran et al. 2013).

There is strong meridional contrast in upper-ocean structure across the Bay of Bengal (Fig. 1; e.g., Vinayachandran et al. 2012). Riverine FW input plays a greater role in the north, where the barrier layer is more prominent than in the south. The formation and evolution of barrier layers, linked to the modulation of vertical mixing and entrainment at the base of the mixed layer, play a major role in setting SST and modulating ocean–atmosphere interactions on a variety of time scales (Vinayachandran et al. 2002). Thin surface mixed layers due to the presence of freshwater enhance the oceanic response to atmospheric forcing. Strong atmosphere–ocean feedback in this region likely plays a

 Denotes content that is immediately available upon publication as open access.

Corresponding author: Luc Rainville, lucrain@uw.edu

DOI: 10.1175/JPO-D-21-0279.1

© 2022 American Meteorological Society. For information regarding reuse of this content and general copyright information, consult the [AMS Copyright Policy](#) (www.ametsoc.org/PUBSReuseLicenses).

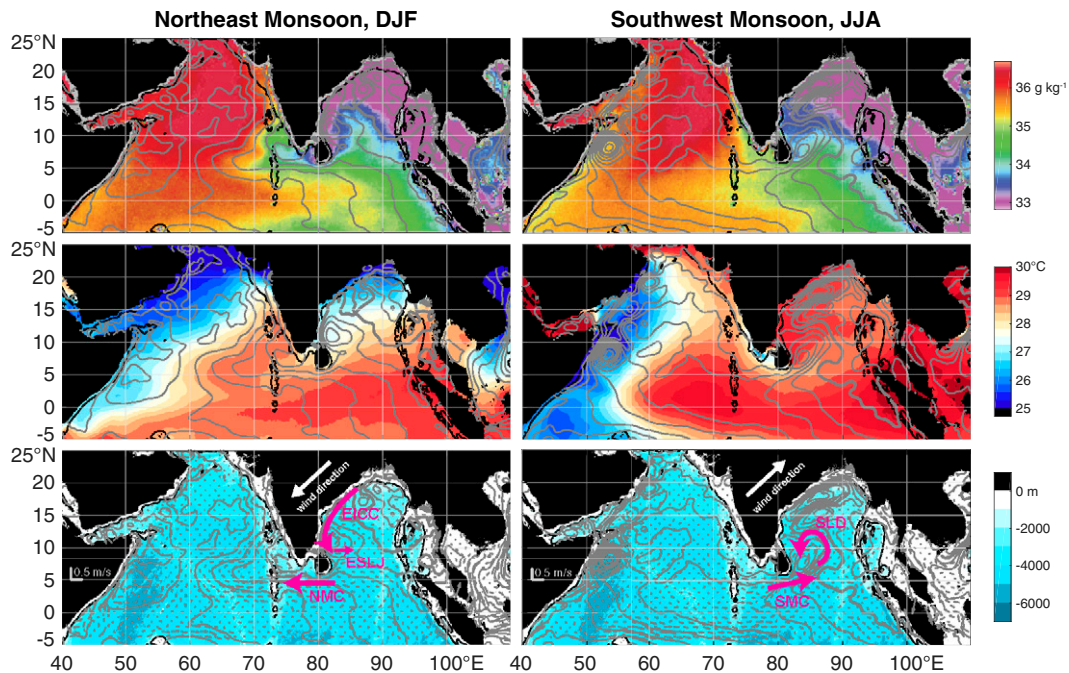


FIG. 1. (top) Maps of surface absolute salinity (from SMAP; Meissner et al. 2018), (middle) temperature (from optimally interpolated microwave and infrared satellites; Wentz et al. 2000), and (bottom) dynamical height and surface currents (from AVISO; Ducet et al. 2000) for the (left) northeast and (right) southwest monsoons. Maps are the seasonal averages for 4 years from 2016 to 2019. In winter, the Northeast Monsoon Current (NMC), East India Coastal Current (EICC), and East Sri Lanka Jet (ESLJ) are labeled. In summer, the Southwest Monsoon Current (SMC) and Sri Lanka Dome (SLD) are labeled.

critical role in determining the properties of water masses exported from the Bay of Bengal and the dynamics of atmospheric disturbances, in particular the monsoon intraseasonal oscillations (MISO) (e.g., Pirro et al. 2020a; Roman-Stork et al. 2020b).

Because it is so variable, the average seasonal circulation of the northern Indian Ocean has been difficult to describe (Shankar et al. 2002; de Vos et al. 2014; Su et al. 2021). Monsoon forcing produces distinctive, seasonal circulation patterns within the Bay of Bengal (Fig. 1). During the northeast monsoon (winter), northeasterly winds drive equatorward flow, carrying fresh Bay of Bengal water south within the East India Coastal Current (EICC). Argo floats, ship-based measurements, SSH, and models show that several eddies are typically positioned off the Sri Lankan coast, deflecting the bulk of the EICC eastward (Fig. 1) to form the East Sri Lanka Jet (ESLJ; Vinayachandran et al. 2005). This forces much of the Bay of Bengal freshwater to take a circuitous eastward path that eventually turns south and west to join the Northeast Monsoon Current [NMC, sometimes referred to as the Winter Monsoon Current (WMC)], the main wintertime communication pathway between the Bay of Bengal and the Arabian Sea. The NMC is further modulated by both coastal Kelvin waves propagating around the Bay of Bengal, and by Rossby waves propagating westward across the Bay of Bengal from the Sumatran coast after the collapse of the southwest (SW) monsoon (Rao et al. 2010; Pirro et al. 2020b; Wijesekera

et al. 2016a). Regardless, the properties of fresher water masses exported out of the Bay of Bengal depend strongly on their exit pathways—whether it is the direct route following the Sri Lankan coast or the more convoluted path through the Bay of Bengal.

During the SW monsoon (summer), southwesterly winds (Fig. 1) reverse the flow between the Arabian Sea and Bay of Bengal (Summer Monsoon Current, SMC) and drive coastal upwelling south of Sri Lanka forming a “mini cold pool” (Vinayachandran et al. 2004; Rao et al. 2006; Pirro et al. 2020a). The SMC entrains this upwelled water, carrying it northeastward into the Bay of Bengal interior. Wind stress curl associated with SW monsoon winds drives Ekman pumping east of Sri Lanka, forming a cyclonic gyre, the Sri Lanka Dome (SLD; Cullen and Shroyer 2019). While the summer monsoon winds drive poleward flow east of India, the western side of the SLD produces equatorward currents along the Sri Lankan coast. Our knowledge of the summer monsoon circulation has recently significantly improved from studies based on direct observations from ship transects (Wijesekera et al. 2015), glider observations in the middle of the Bay of Bengal (Webber et al. 2018), long-term moorings (Wijesekera et al. 2016a), and surface drifters (Hormann et al. 2019), all building on past estimates based on sparse observations. The work presented here complements these snapshots.

Dynamics in the Bay of Bengal and northern Indian Ocean are clearly not one dimensional. Regional numerical simulations

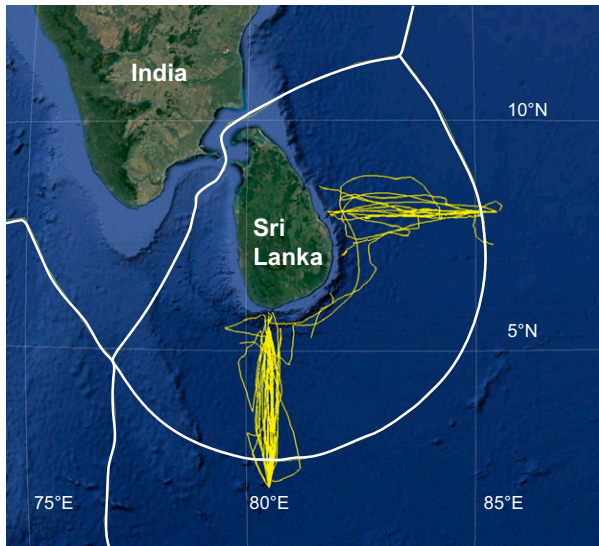


FIG. 2. Map of the Seaglider tracks sampling the circulation around Sri Lanka from December 2013 to December 2019 (yellow). Boundaries of Exclusive Economic Zones are shown in white. Background image from Google Earth.

highlight the interactions of variable winds and currents with local topography, in particular related to enhanced primary productivity in the wake of landmasses (Su et al. 2021). The observations described in this paper describe the variability of the ocean near Sri Lanka, a critical exchange point between the Arabian Sea and the Bay of Bengal. Multiyear glider observations (section 2) are used to describe the seasonal circulation around Sri Lanka including quantification of the mean, seasonal and intra-annual variations of volume, freshwater, and heat transport (section 3).

Discussion (section 4) focuses on understanding the connections between the Bay of Bengal, Arabian Sea, and greater Indian Ocean by tracing the dominant water masses. In particular, we focus on the freshwater exported from the Bay of Bengal, mostly during the northeast monsoon (Fig. 1), which is believed to play an important role in monsoon onset by creating a freshwater pool between the Maldives and India, modulating upper-ocean stratification, forming a barrier layer and a “mini warm pool” that amplifies air–sea feedbacks (Rao et al. 2015; Wijesekera et al. 2016a; Roman-Stork et al. 2020a). Similarly, high-salinity waters from the Arabian Sea entering the Bay of Bengal during the southwest monsoon influences interior stratification and plays a critical role in modulating atmosphere–ocean exchanges (Murty et al. 1992; Vinayachandran et al. 1999, 2018).

2. Data

a. Seaglider

Through a partnership between the Applied Physics Laboratory at University of Washington (APL-UW) and Sri Lanka’s National Aquatic Resources Research and Development Agency (NARA), 15 Seagliders were deployed in

joint operations that began in December 2013 (Fig. 2), conducted as part of the ASIRI (Air–Sea Interactions in the Northern Indian Ocean; Wijesekera et al. 2016b), NASCar (Northern Arabian Sea Circulation–Autonomous Research; Centurioni et al. 2017) and MISO-BOB (Monsoon Intraseasonal Oscillations over the Bay of Bengal; Shroyer et al. 2021) Department Research Initiatives from the Office of Naval Research.

Seagliders are small, reusable, long-range autonomous underwater vehicles designed to glide from the ocean surface to as deep as 1000 m and back while collecting profiles of temperature, salinity, and other oceanic variables with a vertical resolution of about 1 m in the upper part of the water column (Eriksen et al. 2001). Gliders steer through the water by controlling attitude (pitch and roll) and can thus navigate between waypoints to execute survey patterns. In the missions presented here, successive dives (each with a down and up profile) from a glider are generally separated by 4 km and 5 h. Typical horizontal speed is about 20 km day^{−1}. Mission durations depend largely on ambient stratification, profile depth, and instrument power, sometimes extending to nearly a year. Because the vehicles are relatively small and light, special handling gear is not required and field teams typically consist of one or, at most, two individuals. Standard sensor suites include pressure, temperature, and conductivity. Some of the missions near Sri Lanka also included sensors to measure dissolved oxygen, chlorophyll fluorescence, and optical backscatter, but these variables are not discussed here. Seagliders surfaced at the end of every dive cycle, downloading new commands and uploading data to a base station located at the University of Washington via Iridium satellite telemetry.

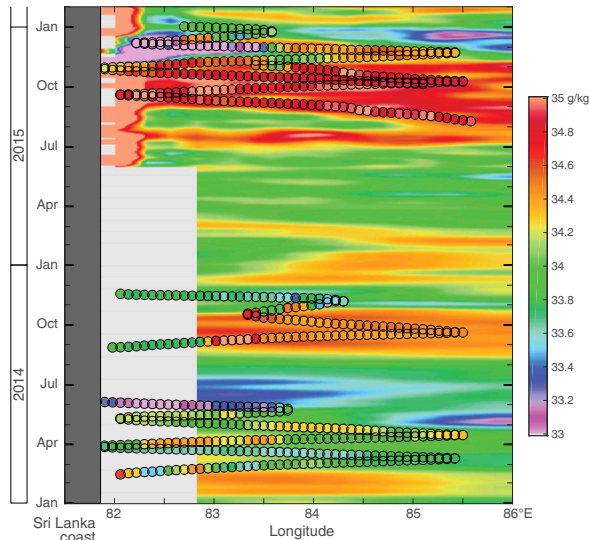
Initial processing is performed in near–real time. The different responses of temperature and conductivity sensors are accounted for and corrected through an analytical physical model (C. Eriksen 2018, personal communication; Morison et al. 1994; Lueck and Picklo 1990) integrated into the base station. A hydrodynamical flight model (Bennett et al. 2019) uses data from the glider’s attitude sensors and from the environment to estimate glider speed through the water, and thus location during the dive. The hydrodynamical model provides an estimate of the horizontal distance traveled through water in an ocean at rest, which, when compared to the actual positions at the beginning and end of the dive, provides a good estimate of the depth-averaged current (or, more accurately, ocean current averaged along the underwater trajectory of the glider). Repeated GPS fixes obtained during the surface drift, before and after every call to the base station, provides an estimate of ocean surface velocity.

Glider deployments and recoveries have taken place near the coasts from R/V *Samuddrika*, NARA’s research vessel, and small local chartered vessels.

b. Satellite remote sensing

Sea surface height products derived from altimetry (Ducet et al. 2000), along with optimally interpolated sea surface temperature (SST) and sea surface salinity (SSS) products, are used for situational awareness during operations and for the

SSS from Aquarius and SMAP (background) and from gliders



SSS from SMAP (background) and from gliders

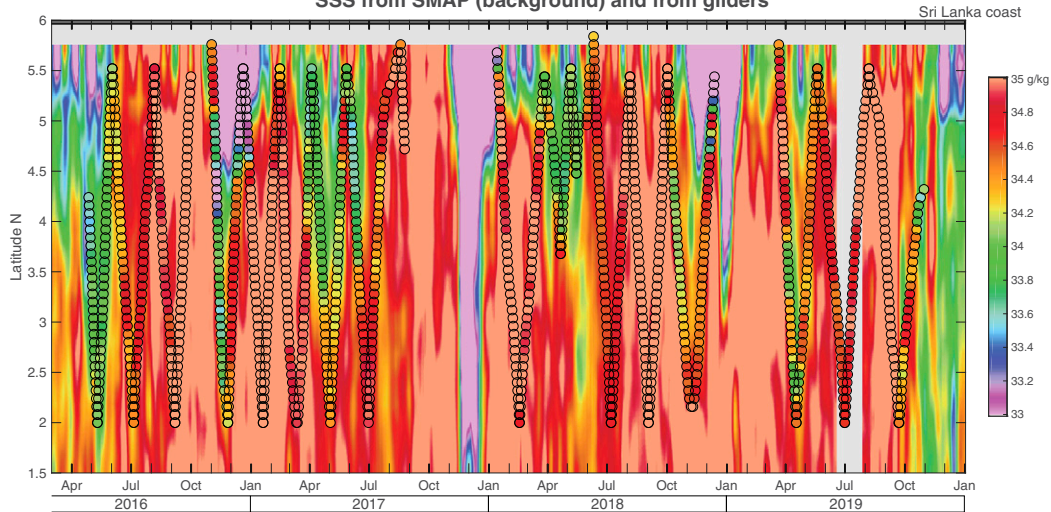


FIG. 3. (a) Map of SSS as a function of longitude and time along 8°N , from the coast of Sri Lanka to 86°E . Background colors are from satellite SSS (Aquarius until June 2015; SMAP after) and from the Seagliders in the black circle. Satellite data are effectively a 120-km running average. (b) As in (a), but SSS as a function of time and latitude along $80^{\circ}30'\text{E}$.

analysis presented here. Absolute dynamical topography is obtained from averaging the sea level anomalies over a prescribed period and adding the MDT_CNES_CLS18 mean dynamical topography (Mulet et al. 2021; also included in the files from Copernicus). SST data are a blended microwave and infrared optimally interpolated product (Wentz et al. 2000). Objectively mapped sea surface salinity from Aquarius resolving features at scales of about 150 km (Melnichenko et al. 2016) is used before June 2015, and from SMAP (Meissner et al. 2018) after April 2015. For SMAP, we use the 40-km v4 product, with an additional running mean filter of 120 km to create a product with similar scales as the Aquarius objective maps. Neither satellite captures the salinity near land, but improvement in the retrieval algorithm for SMAP v4

allows estimates within 30–40 km from the coast (Fig. 3a; Meissner et al. 2019). The general agreement between glider estimates of near-surface absolute salinity (top 5 m, on a 10-km horizontal scale) and satellite products (100-km scale) is encouraging. Direct comparison of the glider surface salinity (top 10 m) and SSS from satellite remote sensing (Fig. 4a) show little systematic bias (the linear regression, in black, has a slope of 0.88 ± 0.01), with a standard deviation of 0.32 g kg^{-1} .

c. Temperature, salinity, and velocity sections

Data collected by Seagliders operating near Sri Lanka can be organized into two sets of sections:

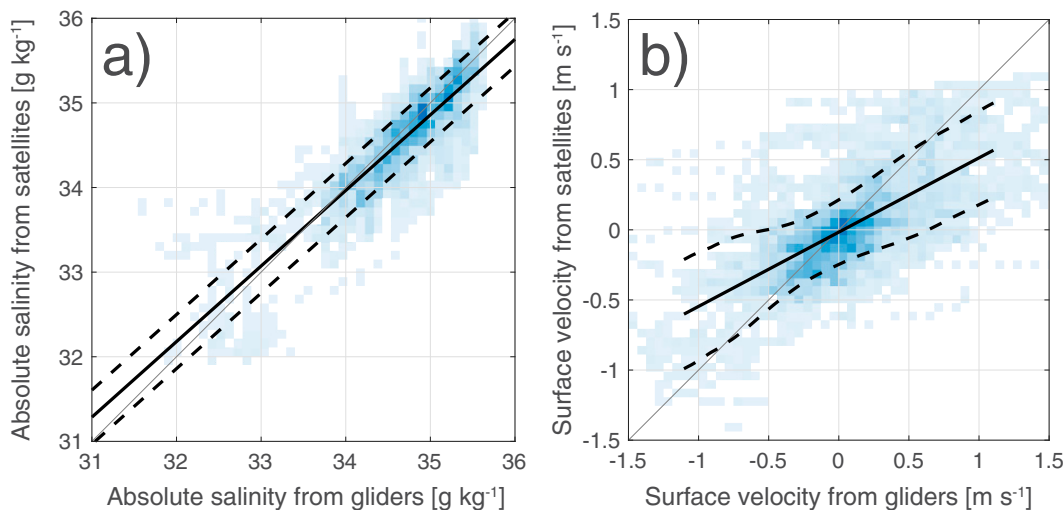


FIG. 4. Scatterplots of (a) glider vs satellite SSS and (b) glider vs satellite surface velocity. Colors provide a relative measure of the number of points. Solid lines are linear regressions and dashed lines show the standard deviation.

- Eastern section (8°N): A zonal section extending offshore at 8°N from the east coast of Sri Lanka. Six missions, conducted between December 2013 and January 2016, completed 17 full and partial occupations of this section, totaling 2243 dives, 433 glider-days (a complete day when a glider is actively sampling) distributed over 751 calendar days, and 7312 km total track distance.
- Southern section (80°30'E): A meridional section extending southward from the southern tip of Sri Lanka at 80°30'E. Five missions, conducted between April 2016 and December 2019, completed 36 full and partial occupations of this section, totaling 3863 dives, 998 glider-days (distributed over 1297 calendar days), and 12 964 km total track distance.

Both sections are roughly 400 km in length, and nominally require 3 weeks for a glider to traverse. Slow occupation speed makes it likely that both temporal and spatial variability contribute to patterns observed along any individual section, necessitating careful choice of scales when interpreting sections for temporal and spatial patterns of circulation and water mass variability.

To facilitate analysis, standard eastern and southern sections are defined as regular grids, with horizontal spacing of 2 km and vertical spacing of 1 m, extending between the nominal end points of each line. For each occupation, temperature and salinity measured along the glider's flight path are mapped onto the standard grid by averaging all observations collected within 10 km horizontally and 5 m vertically of each grid point, effectively smoothing with decorrelation length scales of roughly 10 km (horizontal) and 5 m (vertical).

Geostrophic shear of the horizontal velocity component perpendicular to sections is estimated from the thermal wind equation, i.e., from the horizontal slope of density surfaces. To estimate the absolute geostrophic velocity across the section, careful considerations must be taken in deriving the

reference depth-averaged current. Since small-scale structures are not expected to be in geostrophic balance, the density fields are further smoothed with a 40-km running mean. The uncertainty of individual estimates of depth-averaged currents, typically about 0.1 cm s^{-1} in the cross-track component (much less affected by the parameters derived as part of the flight model calculations, like drag or lift; Bennett et al. 2019) is likely reduced by the spatial average of several dives. Surface drifts, estimated from the glider positions recorded during the 15–20 min period when the glider is at the surface and transmitting its data, and glider-estimated depth average currents from the flight model are smoothed using the same horizontal scale. As the mixed layer can be deep and have significantly different speed than the stratified water, the reference absolute geostrophic in the top 1000 m is calculated by removing (smooth) surface drift over the depth of the mixed layer from the (smooth) depth-averaged currents. The final velocity sections include that same estimate of the surface drift over the depth of the surface mixed layer (assuming no vertical shear in the mixed layer), smoothly transitioning to the interior geostrophic velocity over a depth of 50 m. The velocity estimates are therefore not truly “geostrophic velocity,” but rather an estimate of the “subinertial” velocity across the sections. This technique is similar to adding an Ekman velocity component to the surface (e.g., Centurioni et al. 2009) but does not depend on knowledge of the wind or reanalysis products. Surface velocities from these sections agree relatively well with satellite altimetry products (Fig. 4). Glider estimates are often larger than the satellite estimates, consistent with larger smoothing scales used for the altimetry products. In Fig. 4b, the slope of the regression is 0.53 ± 0.01 for speed less than 1 m s^{-1} , but closer to 0.6 or even higher near zero (not shown), indicating that satellite altimetry often fails to capture large velocities because of the temporal and spatial scales used in the processing (Chelton et al. 2011). Standard deviations (calculated over sliding windows of width 0.5 m s^{-1}) are large,

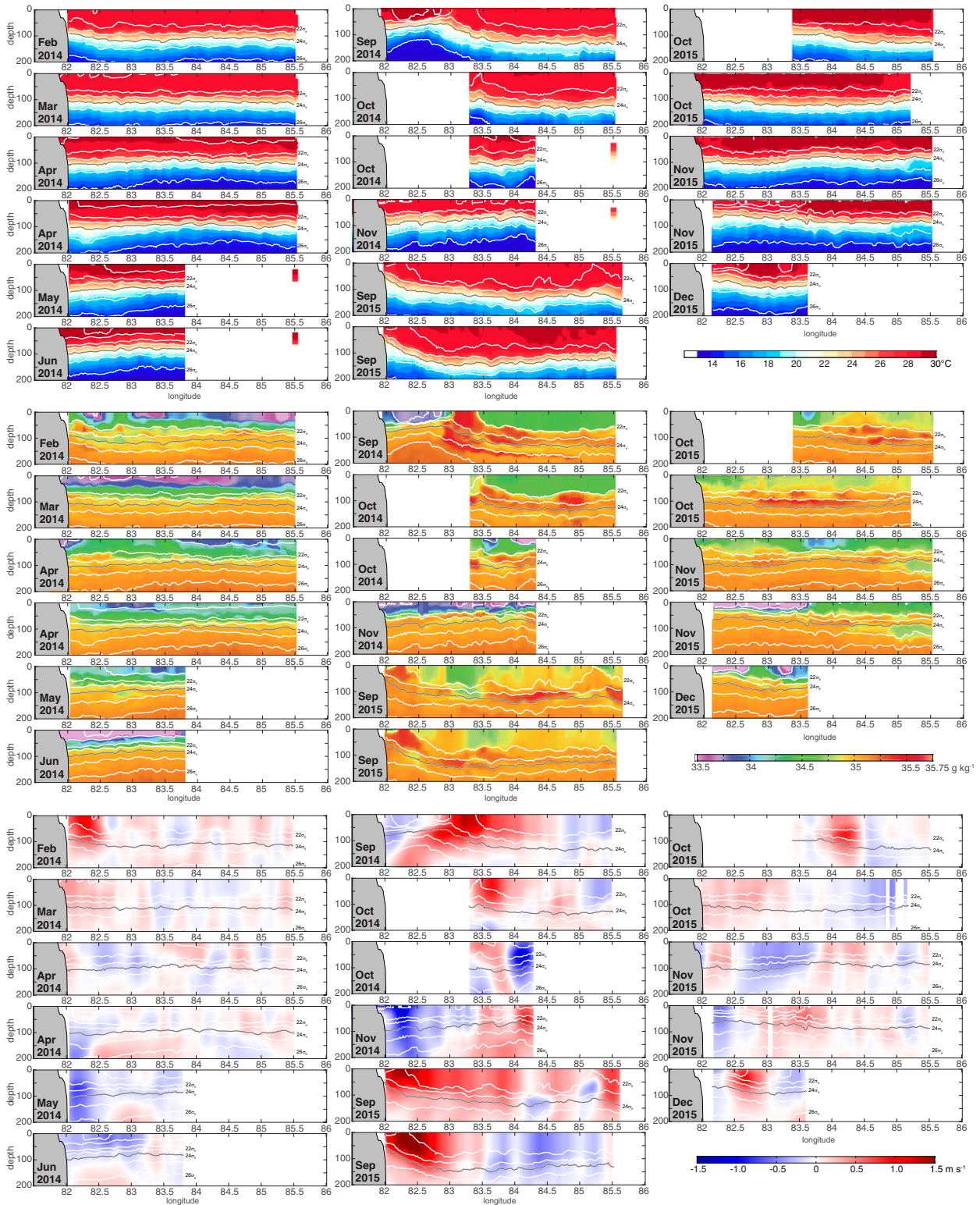


FIG. 5. (top) Upper-ocean temperature, (middle) absolute salinity, and (bottom) northward velocity as functions of longitude and depth for the 17 sections along 8°N. Only the top 200 m (out of 1000 m) are shown.

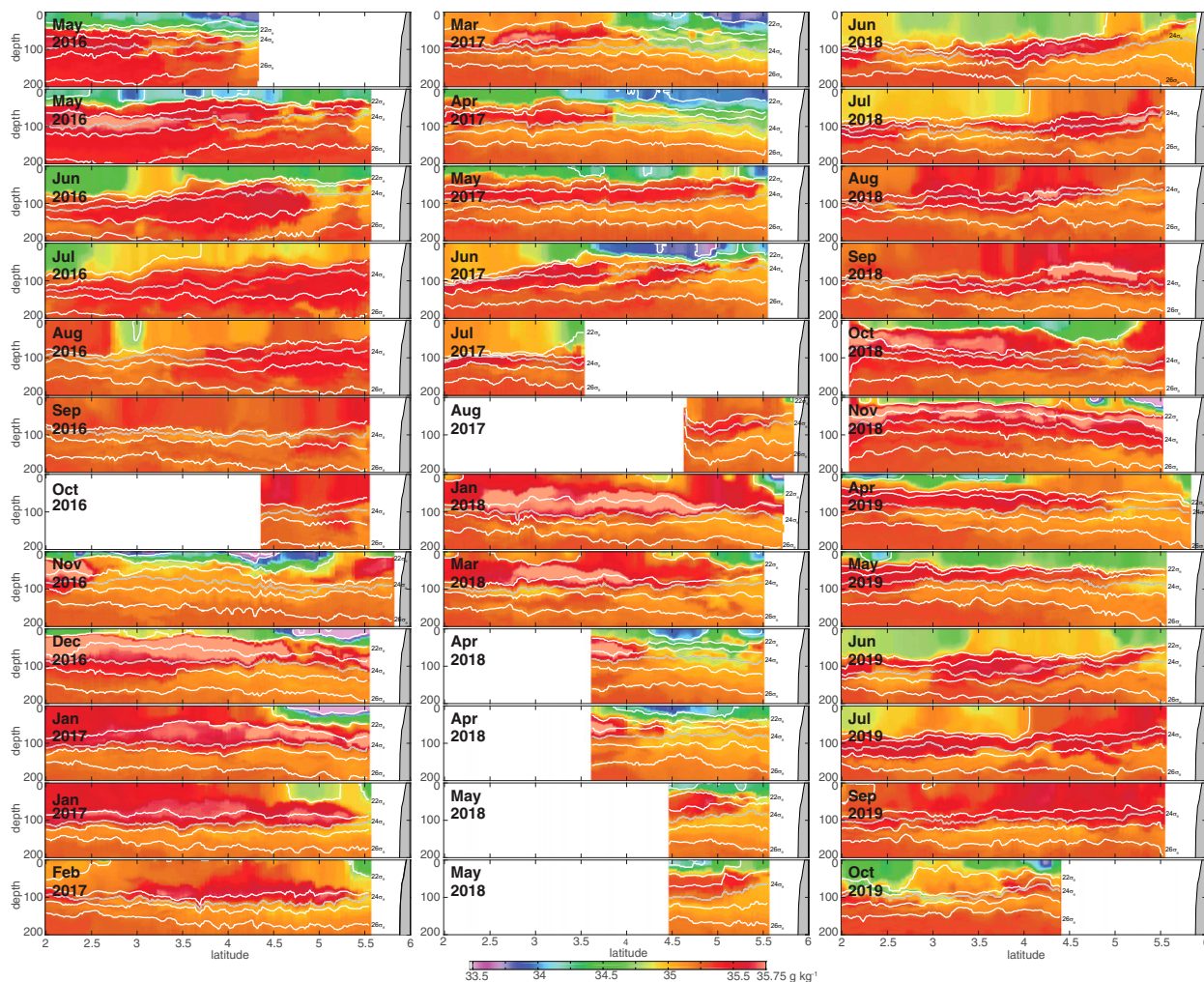


FIG. 6. Upper-ocean absolute salinity as a function of latitude and depth for the 36 sections for the southern section along 80°30'E. Only the top 200 m (out of 1000 m) are shown. Isopycnals are plotted in white (every 1 kg m⁻³, 24σ_θ in light gray).

on the order of 0.35 m s⁻¹. Comparisons with the Ocean Surface Current Analyses Real-Time (OSCAR) surface velocity product (Bonjean and Lagerloef 2002), which include a wind-driven component and arguably a better representation of the ocean surface velocity, lead to very similar results. We note that when comparing the OSCAR velocities evaluated at the glider locations with the same for AVISO, they agreement is much higher with a slope of 0.9 and a standard deviation is 0.21 m s⁻¹. The mismatch between the gliders and both altimetry-based estimates are therefore likely due to intrinsic differences on how the fields are sampled by altimetry and gliders.

1) EASTERN SECTION

Sections along 8°N (Figs. 3a, 5) capture the complex circulation near Sri Lanka, including the narrow southward advection of freshwater near the coast (e.g., September 2014 section) and the subsurface high-salinity water from the Arabian Sea entering the Bay of Bengal (the salty subsurface northward current in fall of each year). Importance

of sampling near the coast is particularly obvious when comparing surface glider observations with estimates from satellites (Fig. 3), where the freshwater near the coast is often missed by remote sensing from space.

Between December 2013 and August 2015, a subsurface mooring was deployed by the United States Naval Research Laboratory at 8°N, 85°30'E, capturing upper-ocean velocity, temperature, and salinity (Wijesekera et al. 2016a). While the mooring provides great temporal resolution of the properties at this location (Pirro et al. 2020a), it minimally contributes to the spatial sections presented here (mooring data appear as a line in Fig. 5, May 2014, October 2014, and November 2014, mostly in temperature). Mooring data are included here for completeness.

The long sampling gap in early 2015 is a direct consequence of the difficulty to get sustained measurements in regions with difficult access. Operations for the 8°N were complicated by the availability of R/V *Samudrika* and access to the port of Trincomalee for political reasons.

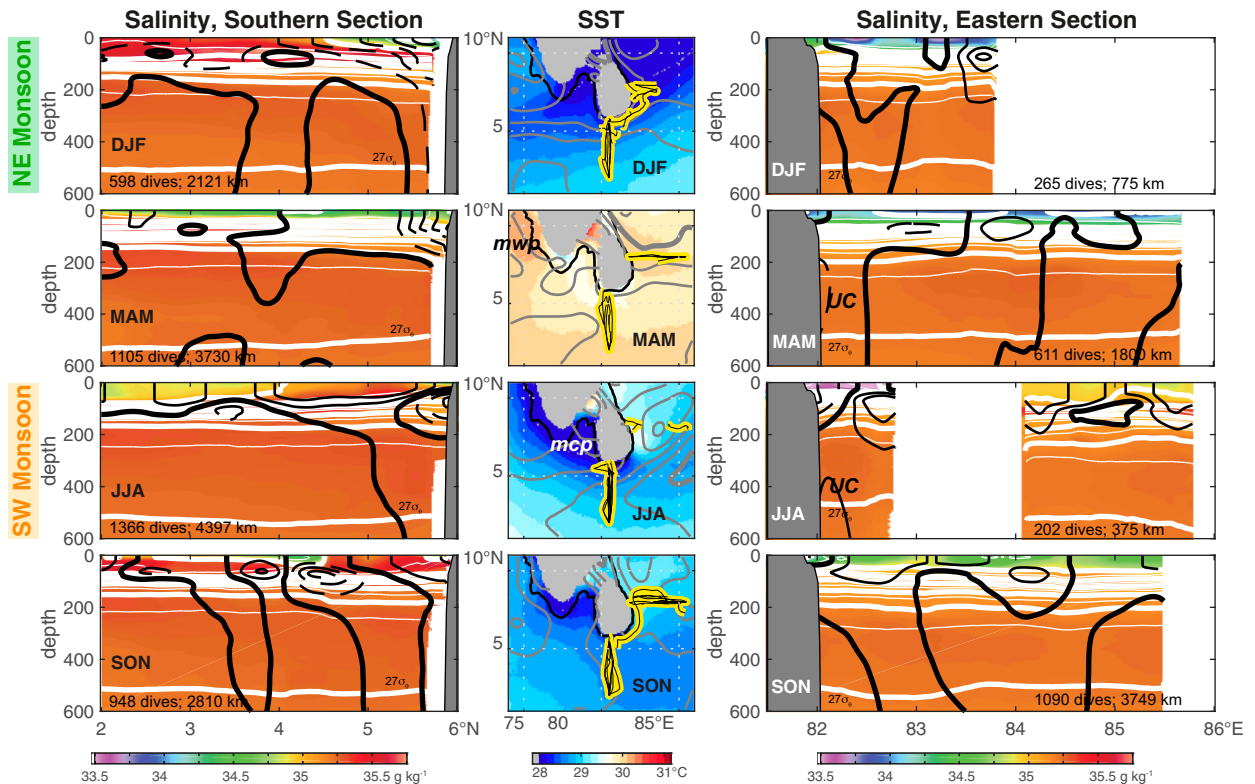


FIG. 7. Seasonal average of the upper-ocean absolute salinity as a function of (left) latitude and depth for the southern section and (right) longitude and depth for the eastern section. Only the top 600 m (out of 1000 m) are shown. The range for absolute salinity is the same for all salinity sections. Isopycnals are plotted in white (thin contours every 0.5 kg m^{-3} , 1 kg m^{-3} in bold). Cross-section velocity is contoured in black [0.5 m s^{-1} intervals; 0 m s^{-1} in bold, positive values (east or north) are solid, negative are dashed]. The Sri Lanka Undercurrent (UC) is indicated. (center) Averaged maps of SST corresponding to the same 3 months, with glider tracks (yellow) and SSH contours (5 cm intervals, gray) overlaid. In italic, the Arabian Sea mini warm pool (mwp) in the spring season is indicated, and the mini cold pool (mcp) in the SW monsoon.

Glider sampling, completing each section in less than a month, is well suited to capture the main modes of variability seen in satellite sea surface salinity, with the direct observations extending closer to the coast in a region important for freshwater export. There is significant seasonal and interannual variability in all fields.

2) SOUTHERN SECTION

Seasonal sampling on the southern section along $80^{\circ}30'E$ (Figs. 3b, 6) is more regular and spans a longer time period than that at $8^{\circ}N$. Some of the sections start near the shelf break at $5^{\circ}50'N$, but operationally the 40-km region between $5^{\circ}30'$ and $5^{\circ}50'N$ was avoided because of heavy ship traffic and fishing activity. Note that the continental shelf south of Sri Lanka is less than 10 km wide (coastline along $80^{\circ}30'E$ is located at $5^{\circ}56'N$).

The southern section exhibits considerable variability across individual occupations. For example, the 36 sections of absolute salinity collected along the southern section (Fig. 6) show strong interleaving of fresh and salty water masses, and narrow filaments of freshwater particularly near the coast, but also throughout the section. Changes

from section to section observed in the glider sections are not unlike the variability observed between a series of ship-based measurements obtained in the early 1990s (Schott et al. 1994).

3. Results

a. Seasonal average of upper-ocean sections

Glider sampling is not uniformly distributed in time, with significant gaps in some seasons. For the southern section, there are at least five complete sections during a given 3-month period, which allows us to calculate a good estimate of the seasonal average from close to the coast of Sri Lanka to $2^{\circ}N$ (Fig. 7). The seasonal cycle measured by the gliders shows the freshwater concentrated near the coast during the winter months, and a variable circulation comparable to that described by numerical simulations of Su et al. (2021) forced with reanalysis winds, emphasizing how reversing monsoon winds and regional bathymetry are responsible for setting up the seasonal circulation around Sri Lanka.

Sparser sampling along $8^{\circ}N$ makes the 3-month average less representative and with more gaps (Fig. 7). Seasonal

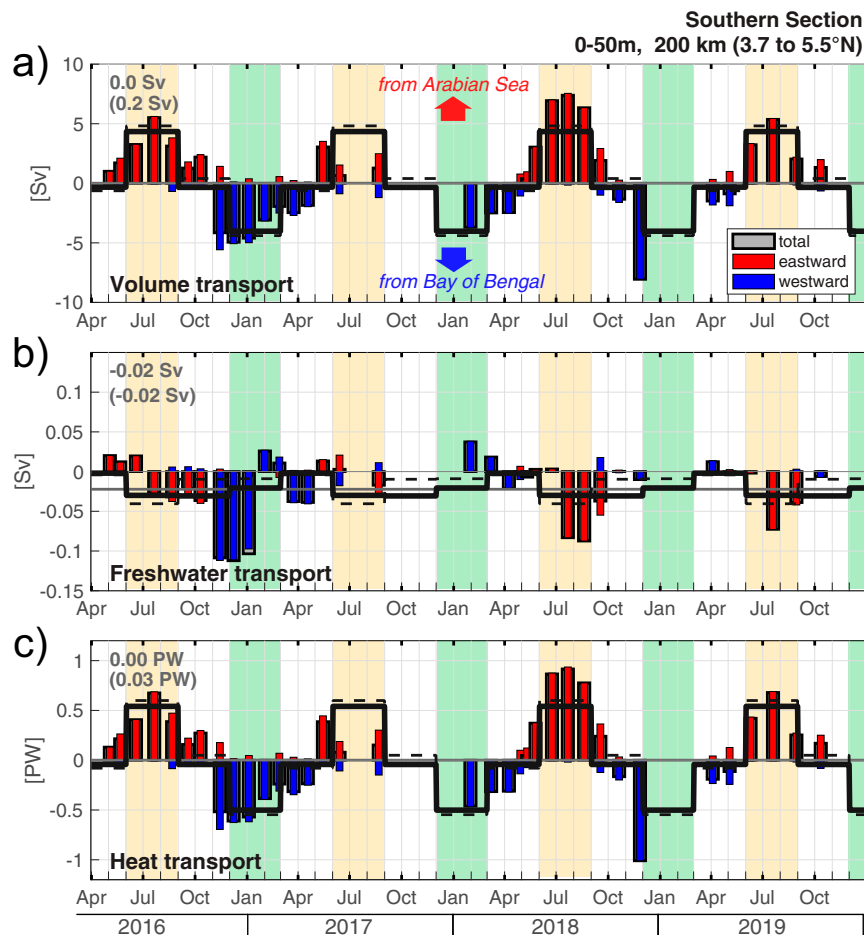


FIG. 8. Time series of the (a) volume, (b) freshwater, and (c) heat transport across the top 50 m and the portion of the southern section within 200 km of the coast, separated by the direction of the flow. Solid black lines indicate the seasonal average of all transports, and dashed lines the transports of the seasonal averages. Annual averages are listed on the top-left corner (transports of the mean sections in parentheses) in gray and illustrated by a constant gray horizontal line.

averages are consistent with previous observations and remote sensing. Freshwater is generally present near the coast of Sri Lanka, particularly in the winter months. Saltier waters are present in the summer months across the whole southern section and offshore in the eastern section, where the end of our observations (near 86°E) connect to where the sampling of Webber et al. (2018) begin—this is where the core of the high-salinity waters of the SMC are detected (Jinadasa et al. 2016).

Even in the seasonal average, sections show horizontal and vertical variability. Velocity and water properties below the surface make it difficult, or impossible, to infer the total transports from only surface properties. As with every individual section, we note that the velocities often reverse at depth. In particular, the undercurrent near the coast of Sri Lanka on the 8°N line, discussed in Anutaliya et al. (2017) based on pressure-inverted echosounders (PIES), models, and a subset of the glider observations presented here, is apparent in both

the seasonal average (particularly during the summer monsoon) and several sections.

Currents are strong in the upper 100–200 m. Low-salinity waters are often found near the coast of Sri Lanka, carried southward in the summer across 8°N and westward across 80°E during almost all seasons. Surface salinities agree well with seasonal averages from satellites, but the section emphasizes how the vertical profiles of salinity change at different places and times.

Signatures of the Sri Lanka Dome, described in more detail in de Vos et al. (2014) and Cullen and Shroyer (2019) and Lozovsky et al. (2019), are not obvious in the averaged sections (Fig. 7, JJA on the eastern section) due to poor sampling. The upward doming of isopycnals associated with the cyclonic Sri Lanka Dome is a bit clearer in the individual sections bracketing the southwest monsoon (e.g., Fig. 5, June and September 2014 sections, with isopycnals being shallowest in the middle of the sections).

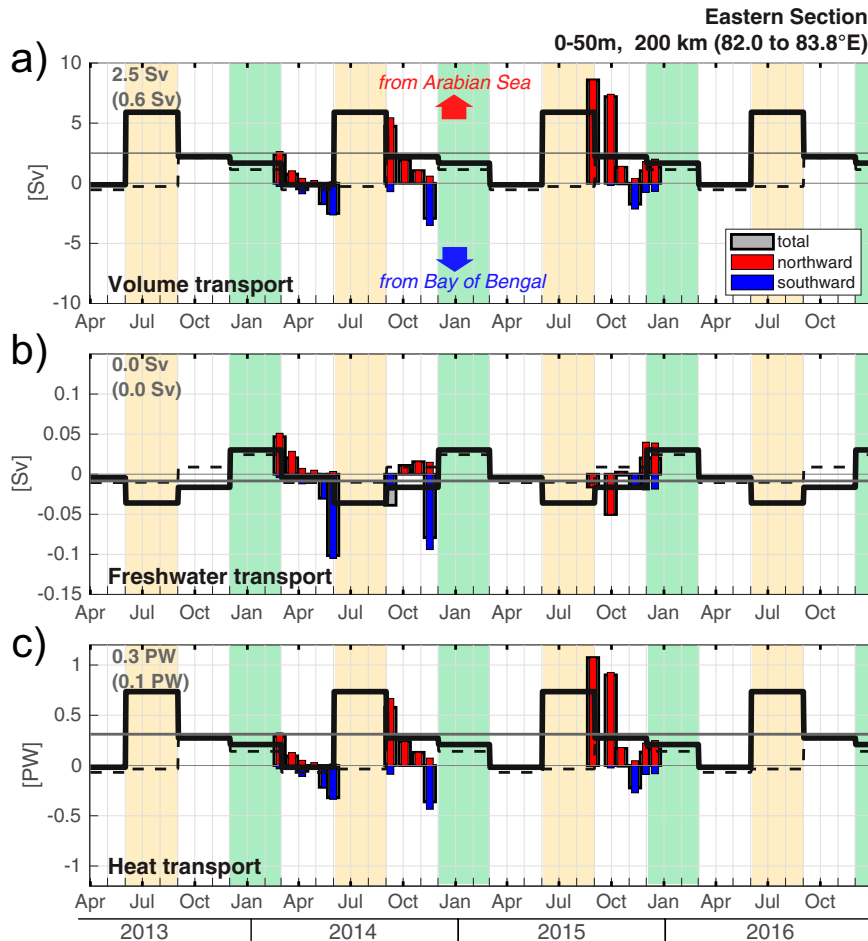


FIG. 9. As in Fig. 8, but for the eastern section within 200 km of the coast.

b. Ocean transport

With the estimates of velocity derived from the glider measurements, an observational estimate of volume, freshwater, and heat transports can be obtained from each section. While salt balance is a fundamental concept for any fixed volume of ocean (or the global ocean, e.g., Talley 2008), several past studies have discussed the concept of “freshwater transport”:

$$T_{FW} = \iint u_{\perp} \left(\frac{S_{\text{ref}} - S}{S_{\text{ref}}} \right) dx dz,$$

which effectively the freshwater fraction transport across a section (double integral) with salinity $S(x, z)$ and velocity component $u_{\perp}(x, z)$ perpendicular to the section, relative to a reference salinity S_{ref} . Reference here is 34.83 g kg^{-1} , corresponding to the same reference salinity for the Indian Ocean used by Roman-Stork et al. (2020a) for their freshwater flux component. The absolute salinity value referred to above is equivalent to 34.67 psu, the mean salinity of the basin. While we acknowledge the limitations and arbitrary nature of the freshwater transport (see, e.g., Schauer and Losch 2019), it is

a useful parameter to describe the net freshening impact of both the northeast and southwest monsoon currents. A more robust metric, namely, the volume transport of water matching specific salinity and density criteria, is presented in section 4.

Along the southern section, positive volume transport indicates water flowing eastward, from the Arabian Sea to the Bay of Bengal. The strongest surface layer transport (Fig. 8a) is negative during the NE monsoon (winter, JJA), and positive during the SW monsoon (summer, JJA), in line with previous observations. The transport estimates match previous estimates, for example the eastward transport of 8 Sv ($1 \text{ Sv} \equiv 10^6 \text{ m}^3 \text{ s}^{-1}$) estimated by Schott et al. (1994) during the SW monsoon north of $3^{\circ}45'N$ along the same meridional section. Other estimates, nicely summarized in Shankar et al. (2002), do vary quite a bit but are consistent with our estimates. Anutaliya et al. (2017) and Anutaliya et al. (2022) find great agreement between the direct (slow) estimates from gliders and those from PIES deployed concurrently to our surveys.

These surface currents generally carry low-salinity waters westward ($S_{\text{ref}} - S > 0$, $u < 0$) during the NE monsoon, and high-salinity water eastward ($S_{\text{ref}} - S < 0$, $u > 0$) during the SW monsoon, resulting in both cases into a negative freshwater

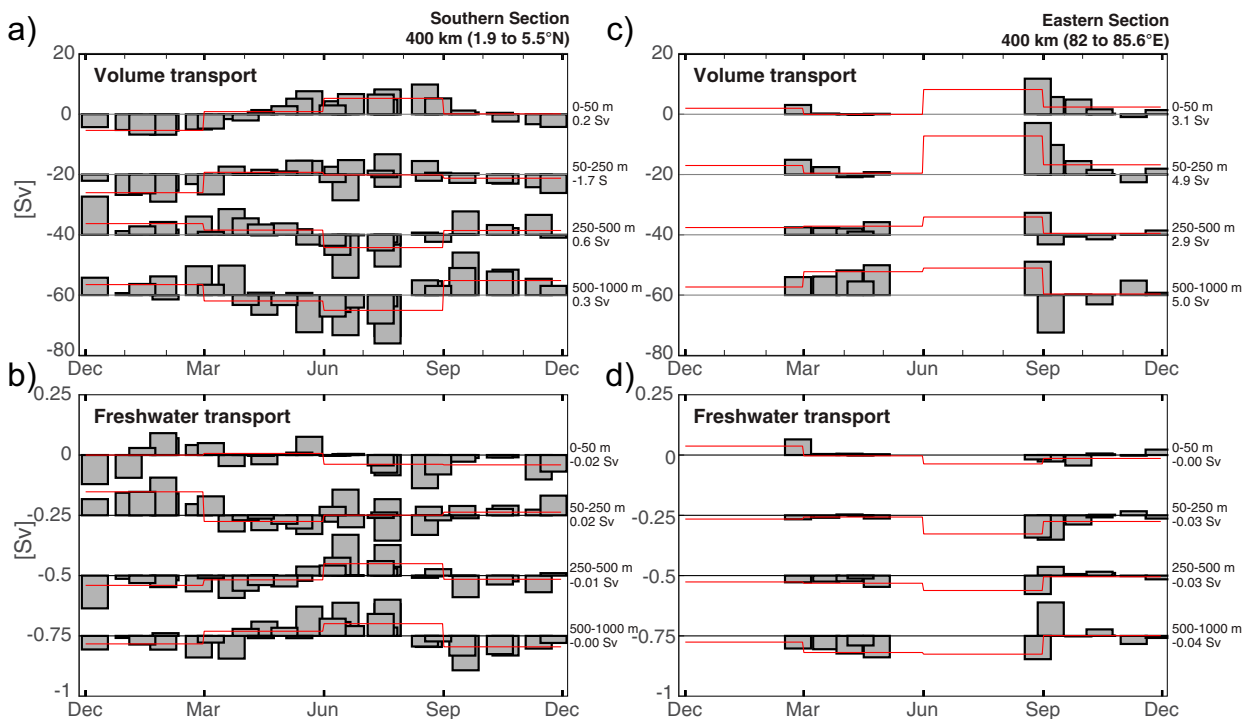


FIG. 10. Time series of the (a),(c) volume and (b),(d) freshwater transport for the (left) southern and (right) eastern sections for four different depth ranges, plotted in terms of year day. Red lines show the seasonal average of transports from individual sections, with the annual average listed on the right.

transport (Fig. 8b). Heat transport (Fig. 8c) are large and follow the volume transports. They are included here for completeness. While interannual variations in the heat transport follows that of the volume transports (e.g., strong eastward volume and heat transport in JJA 2018 vs 2019), the interannual variability of freshwater transport does not follow the same pattern, therefore largely due to salinity anomalies as opposed to current anomalies. Note that transports shown in Figs. 8 and 9 are integrated only in the first 200 km from the coast and any individual section (displayed as a bar) is excluded if less than 75% of that distance is sampled.

Surface transports for the eastern section (Fig. 9) similarly are consistent with the expected seasonal circulation: averaged flow is northward and carries salty waters northward into the Bay of Bengal (negative FW transport, most evident in the average, black line) during the SW monsoon (JJA). Sections closer to the winter monsoon are generally southward and fresh, hence also associated with a negative FW transport. Note that the time span shown for the eastern section (Fig. 9) is the same as for the southern section (Fig. 8) but 3 years earlier, to illustrate how each line is sampled relative to the other and facilitate comparison.

The transports can be calculated for multiple layers, as the gliders provide continuous measurements of the upper 1000 m. Total volume and freshwater transport for several vertical layers, integrated across the entire sections (400 km), are plotted as functions of year day in Fig. 10. Sections from different years often overlap, and the 3-month average for each layer is

shown as the red line. Collapsing the data onto year day obscures interannual trends, instead emphasizing variability and the seasonal cycle.

The vertical structure of the transports is striking (Fig. 10). We note that these four layers have comparable transports despite vastly varying thickness. Transports at depths below 250 m are often opposite to those of the upper ocean. Deeper transports (500–1000 m) are generally in the same direction as those in the 250–500 m depth range.

Both sections (Figs. 8, 9) were sampled for several years, but sampling is uneven. As before, seasonal averages can be calculated for each variable, and these mean salinity and mean velocity sections are used to construct the “transport of the mean sections,” shown as dashed lines in Figs. 8 and 9. Arguably a more accurate measure of the mean transport is obtained by seasonally averaging the transports (solid lines in Figs. 8–10). Discrepancies are mostly due to poor sampling of several seasons (e.g., JJA along eastern section, Fig. 9), but also to the high variability of both salinity and velocity (i.e., the cross terms are important). The net annual volume and heat transports are small for the southern section (Figs. 8a,c, solid gray line and the 0.1 Sv value listed in the top-left corner), but large for the eastern section (Figs. 9a,c), likely due to poor sampling in both monsoon seasons. Throughout the paper, the seasonal mean and standard deviation are calculated from individual sections, weighing the portion of each section that fall within a given 3-month period.

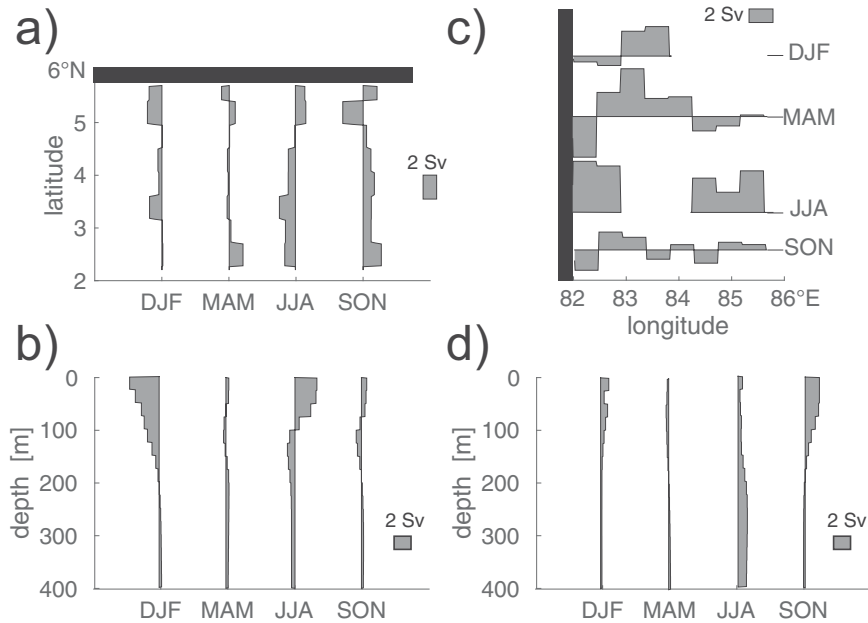


FIG. 11. Seasonal average of volume transports for the southern section as functions of (a) latitude in 50-km bins integrated over the top 250 m, and (b) of depth in 25-m bins integrated over the entire section. Similar seasonal average of volume transports for the eastern section as functions of (c) longitude in 50-km bins integrated over the top 250 m and (d) of depth in 25-m bins integrated over the entire section. Black bars in (a) and (c) represent the coast of Sri Lanka.

Perhaps a simpler way to look at the transport is to average all the transports from each season together. The seasonal average of the volume transports in the top 250 m of the water column in 50-km bins (Figs. 11a,c) show the surface circulation described earlier, where transports are generally westward near the coast of Sri Lanka (southward on the eastern line) except during the summer monsoon (JJA). Seasonal averages of the volume transports also generally reverse direction with depth and show a more complex vertical structure (Figs. 11b,d), most notably during transition periods. Implications of the vertical structure of the current for the import and export of water

TABLE 1. Seasonal average and standard deviation of depth-integrated transports (Sv), over a range of depths and lateral extent, for the southern section. Integral is from 3°42'N to 5°30'N for the 200-km extent and from 2° to 5°30'N for the 400-km values.

	DJF	MAM	JJA	SON
Southern section	5 sections	12 sections	12 sections	7 sections
0–250 m, 200 km	-7.4 ± 3.0	-1.4 ± 4.5	7.4 ± 4.2	-2.6 ± 5.9
0–1000 m, 200 km	-4.5 ± 2.9	-0.6 ± 5.9	0.7 ± 5.9	-1.1 ± 4.3
0–250 m, 400 km	-12.1 ± 3.4	1.6 ± 7.0	5.2 ± 6.1	-1.1 ± 5.6
0–1000 m, 400 km	-4.4 ± 8.2	1.2 ± 8.1	-4.2 ± 14.1	5.2 ± 7.9

masses from the Bay of Bengal and Arabian Sea will be discussed in section 4.

Finally, the total volume transport across the southern section, both for the 200 km closest to Sri Lanka and for the entire 400-km section, are listed in Table 1 for the top 250 m and the top 1000 m in each section. Both directions are integrated to obtain the total transport (positive eastward). The number of sections sampled in each season (over the entire 4-yr period) is listed on the first line. Standard deviation is a measure of the variability between these sections. While the average transports are largest during the monsoon seasons, particularly at the surface, the standard deviation is larger than the mean during the transition period. It is particularly noticeable that standard deviations grow significantly when the deeper depths are included, particularly when the offshore part of the section

TABLE 2. Seasonal average and standard deviation of depth-integrated transports over a range of depths and longitudes, for the eastern section. Integral is from 82.0° to 83°49'E for the 200-km extent and from 82.0° to 85°38'E for the 400-km values. Values are not listed if the coverage is not greater than 75%.

	DJF	MAM	JJA	SON
Eastern section	2 sections	5 sections	1 section	9 sections
0–250 m, 200 km	4.0 ± 1.5	0.5 ± 3.6	50.0	$50. \pm 8.8$
0–1000 m, 200 km	5.8 ± 2.6	11.8 ± 7.1	21.8	3.1 ± 10.4
0–250 m, 400 km	—	0.4 ± 3.9	21.0	5.6 ± 10.0
0–1000 m, 400 km	—	11.0 ± 5.3	35.8	6.5 ± 14.7

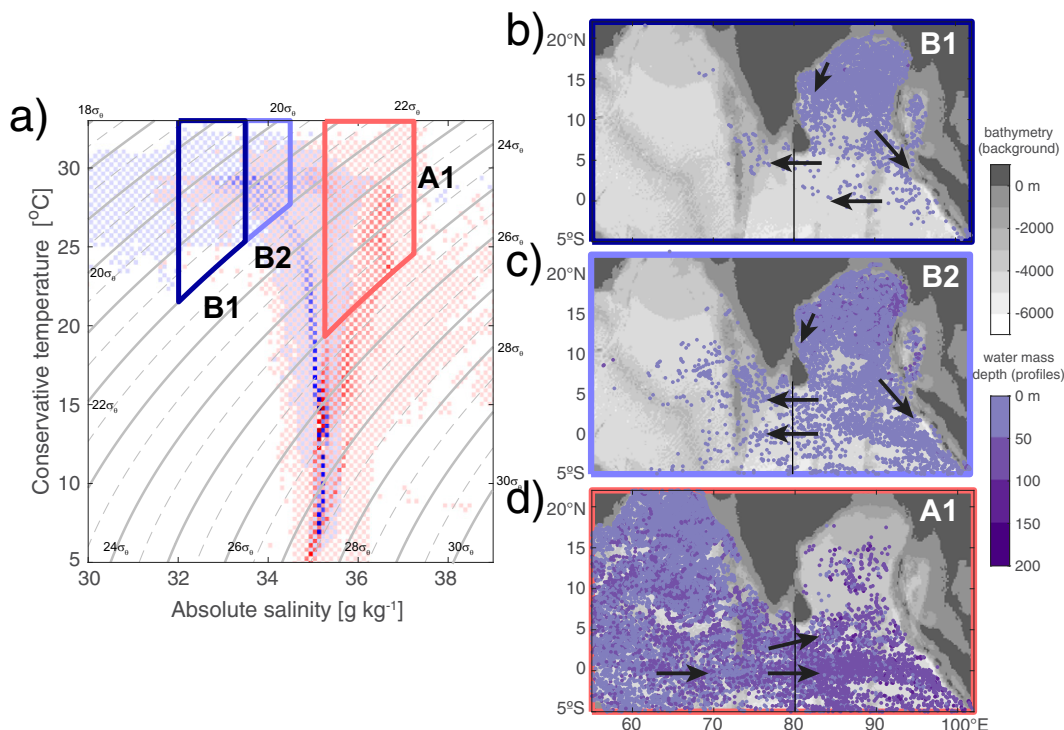


FIG. 12. (a) Temperature–salinity diagram of all Argo float profiles (2016–19) in the Indian Ocean north of 5°S in the Arabian Sea (red) or Bay of Bengal (blue). Each bin is split in two to show the overlap of both density distributions. (b)–(d) Maps of the locations of every float profile, for the entire 4-yr period, with given water mass criteria [boxes in (a)]. For (b)–(d), the color of the dots indicates the depth where the water mass is found (purple color bar) and bathymetry is shaded in gray (gray color bar).

is included. This points to the importance of equatorial dynamics in modulating the circulation.

The equivalent seasonal mean and standard deviation of transports across 8°N are listed in Table 2. Positive values indicate northward flow. The number of sections is significantly smaller, so both mean and standard deviations are less well defined, and some estimates are not possible to make. Generally speaking, the variability is larger than the mean, and individual estimates made from ship-based sections or short-term records are thus unlikely to be representative of the average. While the sampling during summer monsoon is poor, the JJA values are of the same order of magnitude as offshore transport measured during the 2016 Bay of Bengal Boundary Layer Experiment (BoBBLE) field campaign (a northward transport between 16.7 and 24.5 Sv; Webber et al. 2018). At that time the SMC was east of 85°30'E, the limit of the Sri Lankan Exclusive Economic Zone, where our measurements end and those described by Webber et al. (2018) begin. Unfortunately, the 8°N line was not sampled during the period covered by the BoBBLE field campaign. Although there is no good estimate for the northeast (NE) monsoon, transport magnitude and variability in late fall measured by the glider is consistent with the estimates from numerical simulations and the snapshot obtained from a ship in December 2013 at the beginning of the ASIRI program (Wijesekera et al. 2015).

4. Discussion: Transport of specific water masses

Unless sampling defines a closed volume, freshwater and heat transports are ill defined, with results highly dependent on the choice of reference value (e.g., Schauer and Losch 2019). An alternative, as shown in this section, is to characterize exchanges between the basins by quantifying the transport and property changes of individual water masses across the glider sections.

Using 4 years of Argo data (2016–19; overlapping with the sampling of the southern section), the properties of all profiles collected in the Arabian Sea (Fig. 12, in red, shaded by the density of points) overlaps slightly with those from the Bay of Bengal (Fig. 12, in blue). We consider all profiles in the Indian Ocean north of 5°S, and separate the two basins at 80°E (black line in Fig. 12). Note that each T – S pair of the T – S diagram has two juxtaposed colors—a shade of red and a shade of blue, to show the distributions in both basins. Generally speaking, floats stayed in the basin where they were deployed—only 60 floats out of 455 floats with unique identification numbers moved across 80°E. In total, there are 34 429 profiles in the Arabian Sea (from 340 floats), and 17 385 profiles in the Bay of Bengal (from 175 floats).

While there is some overlap, the Bay of Bengal is generally much less salty than the Arabian Sea. The temperature–salinity diagram (Fig. 12a) shows a clear distinction between high-salinity waters formed in the Arabian Sea (red) and the low-

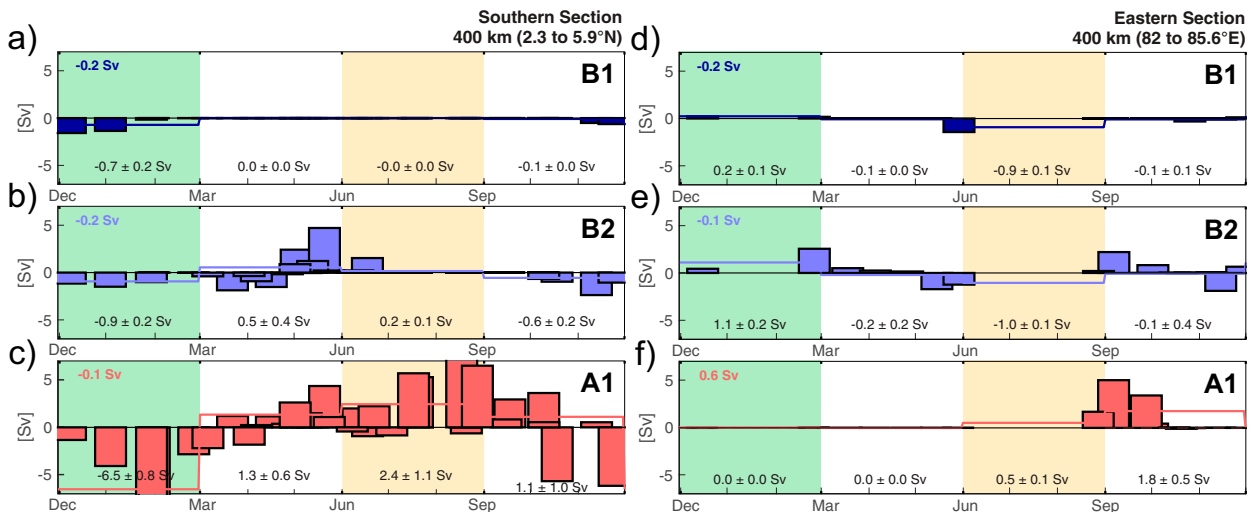


FIG. 13. Transports the B1, B2, and A1 water masses as a function of year day for the (a)–(c) southern section (positive is eastward) and (d)–(f) eastern section (positive is northward).

salinity waters of the Bay of Bengal (blue). Characteristics of three distinct water masses originating from both basins are defined by the density and salinity limits [Fig. 12a; note Hormann et al. (2019) that these are similar to those defined in Hormann et al. (2018), but they use practical salinity units instead of absolute salinity]. Geographically, the fresh Bay of Bengal waters (B1, $32 < S < 33.5 \text{ g kg}^{-1}$; B2, $33.5 < S < 34.5 \text{ g kg}^{-1}$) are mostly present at the northern end of the Bay of Bengal (Fig. 12), with connections on both sides of the Bay. These waters are detected in only a few profiles in the Arabian Sea, with distributions that suggest connections immediately south of Sri Lanka and along the equator (black arrows in Figs. 12b,c). B2 represent a more modified version of the very fresh waters originating from the large rivers of the northern Bay of Bengal, mixed during their transit, and eventually exported to the rest of the Indian Ocean. Similarly, the high-salinity waters (A1, $S > 35.25 \text{ g kg}^{-1}$) are present everywhere in the Arabian Sea, and gradually get deeper toward the east side of the Indian Ocean along the equator and South of Sri Lanka. In the Bay of Bengal, this water mass has been identified as the high-salinity core (HSC), with various direct and indirect links to the Arabian Sea High-Salinity Waters (ASHSW; Jensen et al. 2016; Vinayachandran et al. 1999; Webber et al. 2018; Todd 2020). Locations of Argo profiles that contain these water masses (Fig. 12d) suggest that the high-salinity waters spread in two distinct bands, along the equator and south of Sri Lanka, entering the central Bay of Bengal mostly south of 8°N , below the surface.

These three water masses can be identified directly in each glider section, and its transport is calculated by multiplying each water parcel (with vertical and horizontal extent) meeting these characteristics by their cross-section velocities. Integrating these transports over the whole 400 km sections, the seasonal cycle of the exchange circulation between the basins emerges (Fig. 13). Colors for plotting with each water mass are kept consistent through this section.

A geographical representation of the seasonal transport of these water masses, overlaid with seasonal averages of SSH (Fig. 14), shows that the mean transports obtained by averaging the transports over all sections (solid bars) agree well with the seasonal circulation described above. The fresher water masses (blue) at the surface are dominantly transported near the coast and follow the (wind-driven) geostrophic circulation inferred by altimetry, as does modified Arabian Seawater (red) particularly during the SW monsoon. Estimates from individual sections often show transport in the opposite direction than the average.

The vertical structure of the transport of these three water masses is plotted in Fig. 15. The fresh B1 and B2 water masses are confined to the surface (top 25 m), which has allowed previous studies to obtain accurate estimate of freshwater transports from remote sensing (e.g., Roman-Stork et al. 2020b) or surface drifters (e.g., Hormann et al. 2019). High-salinity waters from the Arabian Sea have a more complex vertical distribution, extending from the surface to over 100 m, often with subsurface maximum.

Based on the analysis of particle release experiments in an assimilation model, Sanchez-Franks et al. (2019) propose that the high-salinity core in the Bay of Bengal is linked to the Equatorial Undercurrent (EUC), originating in the western Indian Ocean. Similar connections have been made using data from surface drifters (Hormann et al. 2019) and gliders (Todd 2020). While no mechanism has been identified to export this water out of the EUC and into the Bay of Bengal, these studies suggest that the main pathways for Arabian Seawater entering the Bay is along the equator, i.e., not much high-salinity water transits north of 2°N along 80°E in either NEMO (Sanchez-Franks et al. 2019, their Fig. 2) or in surface drifters coming from the Arabian Sea (Hormann et al. 2019, their Fig. 3). In contrast, our observations, other models (e.g., Jensen et al. 2016), and earlier work (e.g., Vinayachandran et al. 1999) suggest that the pathway closer to Sri Lanka is

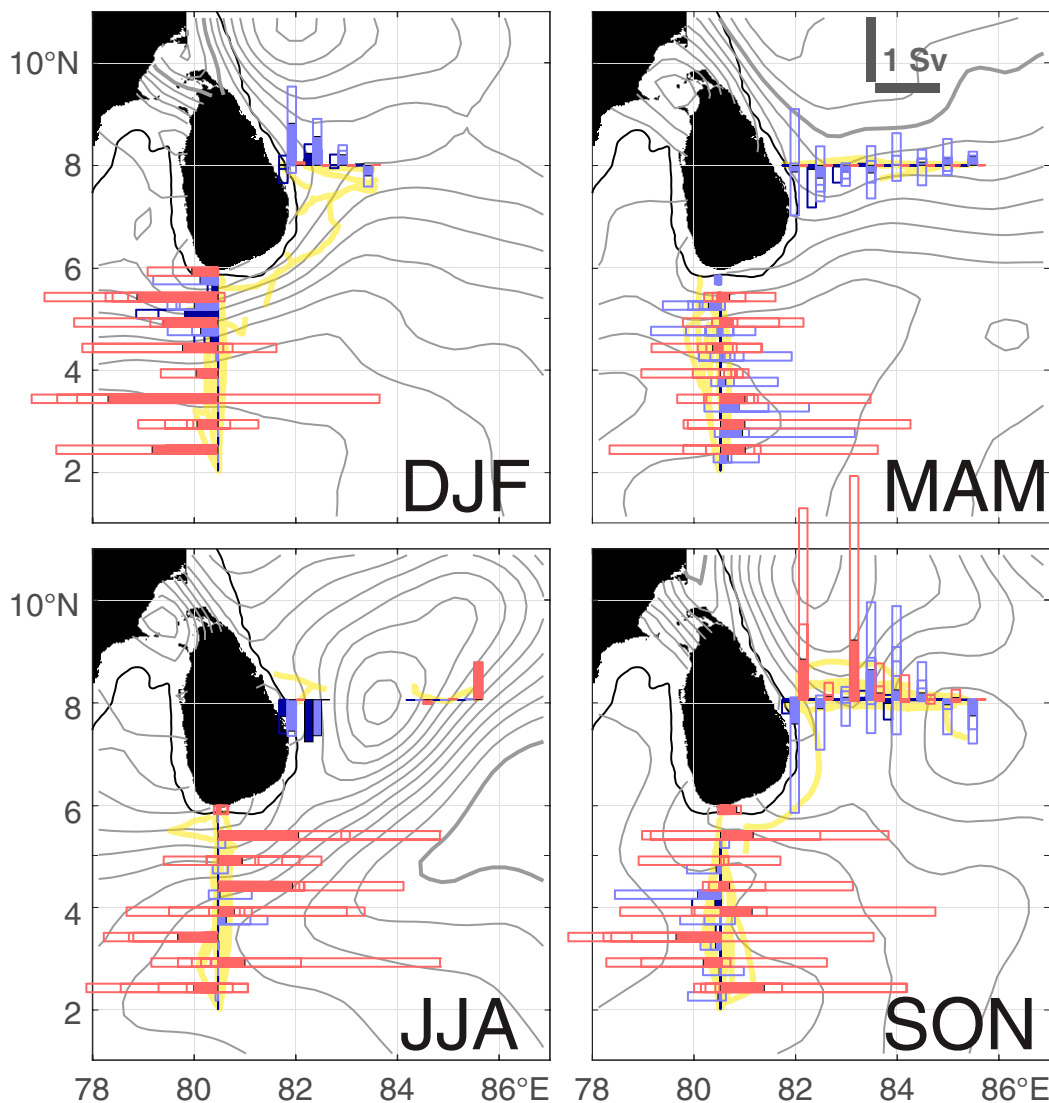


FIG. 14. Seasonal circulation of water masses [salty waters from the Arabian Sea (A1), in red; freshwaters from the Bay of Bengal (B1 and B2), in blue] captured by the gliders over several years, overlaid on the mean SSH contours (2.5-cm intervals) for each season. 1000-m isobath is shown in black. Seasonal mean transports are shown by the solid bars (over all years), and open bars represent estimates from individual sections, in the direction they are transported. Yellow lines show the glider tracks for each season.

important. While the interannual variability of the EUC is likely very important in controlling how and in what volume the high-salinity waters from the Arabian Sea enter the Bay of Bengal, it appears likely that filaments, instabilities, and other processes happening near the Maldives and the southern tip of India play a dominant role for salt transport into the Bay of Bengal. Even in models, the relative importance of these pathways is unclear. More work, including but not limited to the data presented here, will provide insight in this broader circulation.

Interannual monsoon variability

Across the well-sampled $80^{\circ}30'E$ line south of Sri Lanka, the transport across each section sampled by the gliders as

a function of time, for each of the three water masses (Fig. 16), shows interannual, seasonal, and intraseasonal variability are well captured. As seen above and in Fig. 16, the general monsoon circulation can be deciphered from all the sections: there is enhanced transport of high-salinity waters by SMC in the SW monsoon (season marked with the orange background), and westward transport of low-salinity waters by NMC during the NE monsoon (periods with green background).

The probability density functions (PDFs) of salinity in the top 150 m (Fig. 17) show the presence of low-salinity water in all seasons. Different colored lines in the figure show different years. The freshwater transports (B1, B2) emphasized above

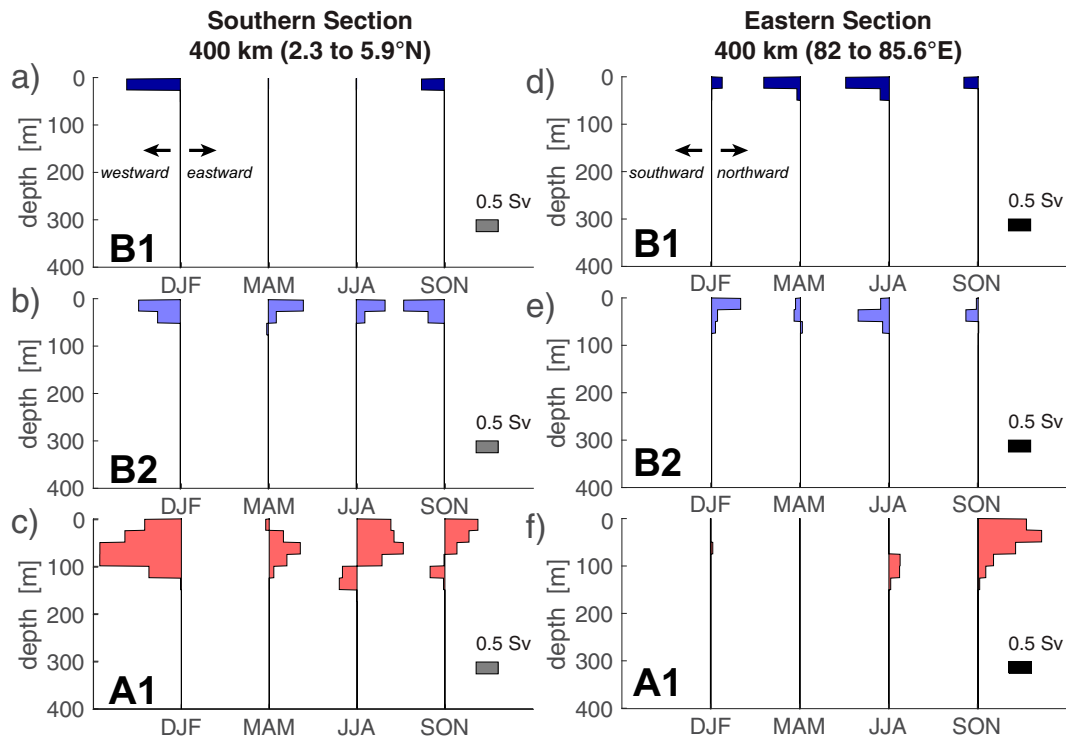


FIG. 15. Transport of water with the properties of water masses (a),(d) B1, (b),(e) B2, and (c),(f) A1 as a function of depth in 25-m bins integrated over the whole section (400 km) for each season for the (left) southern section and (right) eastern section.

are associated with the very low-salinity waters (found near the coast of Sri Lanka), which are quickly advected westward, primarily during the NE monsoon (DJF). The PDFs show that there is proportionally more freshwater in the transition seasons (MAM in particular), but it is more distributed and advected in both directions (see Fig. 14).

There is significant interannual variability. The distributions of both low-salinity waters (blue box in Fig. 17) and high-salinity waters (red box in Fig. 17) changes from year to year, suggesting that the water observed south of Sri Lanka has taken different paths and been modified by different processes. For example, focusing on the last two SW monsoon periods (Fig. 16), there are larger transport of high-salinity waters in 2018 relative to 2019, despite the PDF showing a bit more of salty waters in 2019 (Fig. 17c). This interannual variability is not surprising, particularly given that the ocean conditions around Sri Lanka respond to both local winds (e.g., de Vos et al. 2014) and the timing of annual Rossby waves, linked to Kelvin wave propagating along the equatorial ocean waveguide (Shankar et al. 2002; Rao et al. 2010), both of which are highly variable from year to year.

While a full interpretation of the interannual variability of the circulation presented here requires a much broader perspective, it is worth noting that in 2019 the Sri Lanka Dome was much smaller relative to other years, as seen by the time series of SSH in middle of the mean location of the SLD (Fig. 16e). The SLD is a large cyclonic circulation that develops east of Sri

Lanka during the summer months. Strength and evolution have been linked to the local wind stress, regional forcing and Rossby wave propagation (Vinayachandran and Yamagata 1998; Cullen and Shroyer 2019; Pirro et al. 2020a). The seasonal SSH minimum centered in July (Fig. 16e) is the signature of the SLD. SSH anomalies are negative in 2018 (strong SLD, and large transport of high-salinity water) but positive in 2019 (weak SLD). The data presented here, along with measurements from other sources (e.g., Anutaliya et al. 2017; Hormann et al. 2019; Anutaliya et al. 2022) can be used to explore potential connections between SMC transport south of Sri Lanka and Sri Lanka Dome strength.

5. Summary

Six years of repeated observations, with autonomous gliders collecting over 12 000 profiles along two sections extending south and east from the Sri Lankan coast quantify seasonal variability in the boundary circulation and exchange between the Bay of Bengal and Arabian Sea. The boundary currents within a few hundred kilometers of Sri Lanka carry significant fresh and high-salinity waters between the Arabian Sea and the Bay of Bengal. In addition to reversing with the monsoon winds, this circulation is highly variable at seasonal and interannual time scales, with significant vertical structure (Jensen et al. 2016)

Currents are surface intensified, as observed previously (e.g., Schott et al. 1994), but also show significant vertical

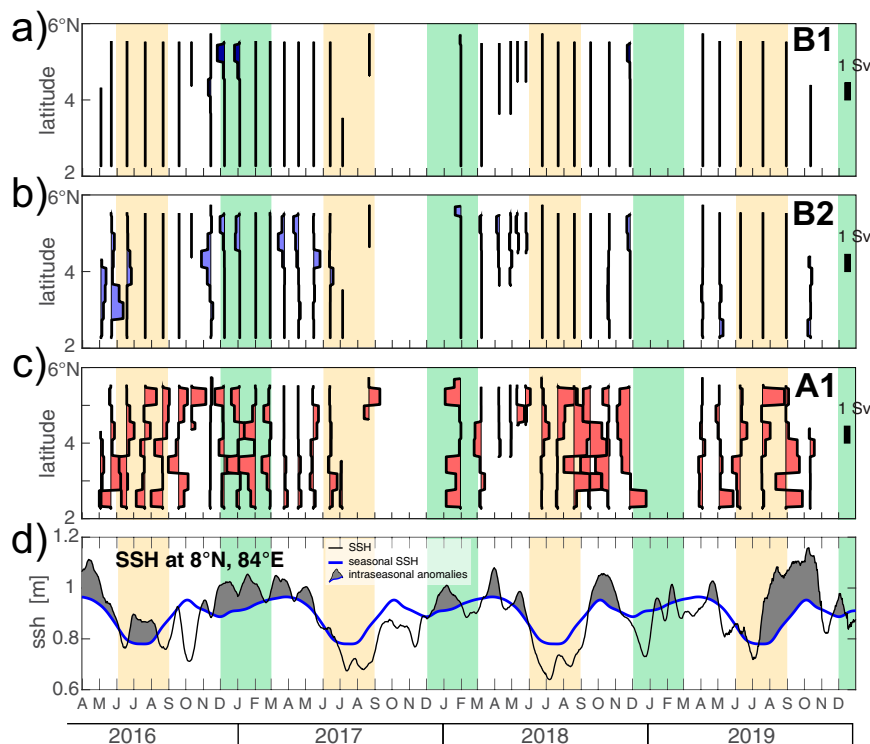


FIG. 16. Transport of water with the properties of water masses (a)–(c) B2, B1, and A1 for all sections across 80.5°E as a function of yearday and latitude (in 50-km bins). (d) Sea surface height time series in the middle of the Sri Lanka Dome, with the 10-yr seasonal average (blue) and positive intra-annual anomalies highlighted.

structure. Flows often reverse with depth, such that subsurface transports of high-salinity waters oppose those in the surface layer. This introduces uncertainty to transports inferred from surface currents and water mass properties. The region south of Sri Lanka, but north of the Equatorial Undercurrent (roughly 2°N) appears to be a dominant pathway for high-salinity Arabian Sea waters entering the Bay of Bengal. While this differs from the pathways recently proposed by Sanchez-Franks et al. (2019), it suggests that circulation in the southeast Arabian Sea (e.g., Lakshadweep eddy, upwelling near the Maldives; de Vos et al. 2014; Pirro et al. 2020b) likely plays an important role in modulating the import of high-salinity water into the Bay of Bengal. The glider estimates of transport are a good step toward quantifying the relative importance of the various pathways of water exchange in the northern Indian Ocean.

As noted previously, the freshwater export during the NE monsoon and spring (MAM) from the Bay of Bengal plays an important role in setting up the upper-ocean stratification in the southeast Arabian Sea (mini warm pool between the Maldives and India; Fig. 7), which is linked to SST and the onset of the SW monsoon (e.g., Roman-Stork et al. 2020a). Irregular sampling and the relatively short 3-yr period covered by gliders make it difficult to draw conclusions from glider data alone, but the results presented should be used to better understand the connections between upper-ocean variability in the southeast

Arabian Sea and the circulation pattern near Sri Lanka. A comprehensive analysis can be conducted by combing with model outputs in future studies, but it is out of the scope of the present paper.

The extensive time series of glider-based observations presented here were one component of a sequence of broad, collaborative, international programs supported by the U.S. Office of Naval Research. These programs provide an unprecedented wealth of sustained observations and focused process studies (Wijesekera et al. 2016b; Centurioni et al. 2017; Anutaliya et al. 2017; Hormann et al. 2019) which, when combined with remotely sensed sea surface height, temperature, and salinity, offer new opportunities to advance understanding of the variability and underlying dynamics of circulation around Sri Lanka.

Acknowledgments. We are grateful to Ben Jokinen, Jason Gobat, and Geoff Shilling (APL-UW), as well to Indika Weligamage and Upul Adikari (NARA) for their invaluable support during field operations. Glider deployments and recoveries in Sri Lanka would not have been possible without the support of NARA's chairmen and ministers. This work has benefited from discussions with Uwe Send, Verena Hormann, Luca Centurioni, Arnold Gordon, and many other investigators involved in the ASIRI, MISO-BOB, and NASCar projects. This work was supported by

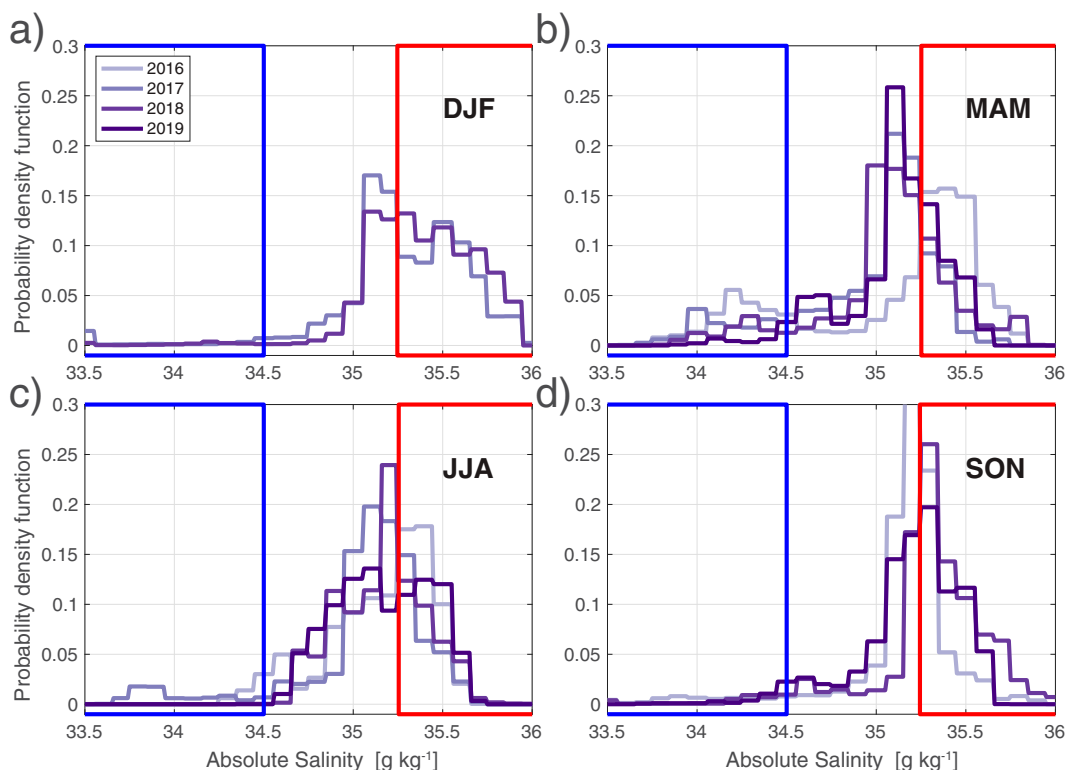


FIG. 17. Probability density function of the salinity along the southern section in the top 150 m from 2° to 5°30'N, for each year and season. Blue and red boxes show the limits of the B2 and A1 water masses, respectively.

the Office of Naval Research, primarily under Grants N00014-13-1-0478, N00014-15-1-2231, and N00014-17-1-2718. The work at NARA and University of Notre Dame was funded by ONR Grant N00014-17-1-2334. Microwave OI SST and SSS data are produced by Remote Sensing Systems and sponsored by National Oceanographic Partnership Program (NOPP) and the NASA Earth Science Physical Oceanography Program.

Data availability statement. The gridded sections and seasonal averages obtained from the Seaglider data presented in this paper are available at the University of Washington Digital Library (<http://hdl.handle.net/1773/48130>). The glider data can be downloaded from the IOP group (Lee and Rainville) website (<https://iop.apl.washington.edu>). Remote sensing SST and SSS are available at www.remss.com. Maps of sea surface height and currents were produced and distributed by the Copernicus Marine and Environment Monitoring Service (CMEMS) (<https://doi.org/10.48670/moi-00148>).

REFERENCES

- Anutaliya, A., and Coauthors, 2017: An undercurrent off the east coast of Sri Lanka. *Ocean Sci.*, **13**, 1035–1044, <https://doi.org/10.5194/os-13-1035-2017>.
- , and Coauthors, 2022: Seasonal and year-to-year variability of boundary currents and eddy salt flux along the eastern and southern coasts of Sri Lanka observed by PIES and satellite measurements. *J. Phys. Oceanogr.*, <https://doi.org/10.1175/JPO-D-22-0030.1>, in press.
- Bennett, J., F. Stahr, and C. Eriksen, 2019: Determining Seaglider velocities automatically. Tech. Rep., Dept. of Oceanography, University of Washington, 50 pp., <https://digital.lib.washington.edu/researchworks/handle/1773/44948>.
- Bonjean, F., and G. S. E. Lagerloef, 2002: Diagnostic model and analysis of the surface currents in the tropical Pacific Ocean. *J. Phys. Oceanogr.*, **32**, 2938–2954, [https://doi.org/10.1175/1520-0485\(2002\)032<2938:DMAOT>2.0.CO;2](https://doi.org/10.1175/1520-0485(2002)032<2938:DMAOT>2.0.CO;2).
- Centurioni, L. P., P. N. Niiler, and D.-K. Lee, 2009: Near-surface circulation in the South China Sea during the winter monsoon. *Geophys. Res. Lett.*, **36**, L06605, <https://doi.org/10.1029/2008GL037076>.
- Centurioni, L. R., and Coauthors, 2017: Northern Arabian Sea Circulation-Autonomous Research (NASCAR): A research initiative based on autonomous sensors. *Oceanography*, **30**, 74–87, <https://doi.org/10.5670/oceanog.2017.224>.
- Chelton, D. B., M. G. Schlax, and R. M. Samelson, 2011: Global observations of nonlinear mesoscale eddies. *Prog. Oceanogr.*, **91**, 167–216, <https://doi.org/10.1016/j.pocean.2011.01.002>.
- Cullen, K., and E. Shroyer, 2019: Seasonality and interannual variability of the Sri Lanka Dome. *Deep-Sea Res. II*, **168**, 104642, <https://doi.org/10.1016/j.dsr2.2019.104642>.
- de Vos, A., C. Pattiaratchi, and E. Wijeratne, 2014: Surface circulation and upwelling patterns around Sri Lanka. *Biogeosciences*, **11**, 5909–5930, <https://doi.org/10.5194/bg-11-5909-2014>.

- Ducet, N., P. L. Traon, and G. Reverdin, 2000: Global high-resolution mapping of ocean circulation from TOPEX/Poseidon and ERS-1 and -2. *J. Geophys. Res.*, **105**, 19477–19498, <https://doi.org/10.1029/2000JC900063>.
- Eriksen, C., T. Osse, R. Light, T. Wen, T. Lehman, P. Sabin, J. Ballard, and A. Chiodi, 2001: Seaglider: A long-range autonomous underwater vehicle for oceanographic research. *IEEE J. Oceanic Eng.*, **26**, 424–436, <https://doi.org/10.1109/48.972073>.
- Hormann, V., L. R. Centurioni, and A. L. Gordon, 2019: Freshwater export pathways from the Bay of Bengal. *Deep-Sea Res. II*, **168**, 104645, <https://doi.org/10.1016/j.dsr2.2019.104645>.
- Jensen, T. G., H. W. Wijesekera, E. S. Nyadjro, P. G. Thoppil, J. F. Shriver, K. K. Sandeep, and V. Pant, 2016: Modeling salinity exchanges between the equatorial Indian Ocean and the Bay of Bengal. *Oceanography* **29**, 92–101, <https://doi.org/10.5670/oceanog.2016.42>.
- Jinadasa, S. U. P., I. Lozovatsky, J. Planella-Morató, A. Lucas, J. MacKinnon, J. Nash, H. W. Wijesekera, and H. J. S. Fernando, 2016: Ocean turbulence and mixing around Sri Lanka and in adjacent waters of the northern Bay of Bengal. *Oceanography*, **29**, 170–179, <https://doi.org/10.5670/oceanog.2016.49>.
- Lozovatsky, I., H. J. S. Fernando, S. U. P. Jinadasa, A. Pirro, H. W. Wijesekera, and E. Jarosz, 2019: Turbulence at the periphery of Sri Lanka Dome. *Deep-Sea Res. II*, **168**, 104614, <https://doi.org/10.1016/j.dsr2.2019.07.002>.
- Lueck, R. G., and J. J. Picklo, 1990: Thermal inertia of conductivity cells: Observations with a sea-bird cell. *J. Atmos. Oceanic Technol.*, **7**, 756–768, [https://doi.org/10.1175/1520-0426\(1990\)007<0756:TIOCCO>2.0.CO;2](https://doi.org/10.1175/1520-0426(1990)007<0756:TIOCCO>2.0.CO;2).
- Meissner, T., F. J. Wentz, and D. M. Le Vine, 2018: The salinity retrieval algorithms for the NASA Aquarius version 5 and SMAP version 3 releases. *Remote Sens.*, **10**, 1121, <https://doi.org/10.3390/rs10071121>.
- , —, A. Manaster, and R. Lindsley, 2019: Remote sensing systems SMAP ocean surface salinities [level 2C, level 3 running 8-day, level 3 monthly], Version 4.0 validated release. PO.DAAC, accessed 9 October 2019, <https://doi.org/10.5067/SMP40-3SPSC>.
- Melnichenko, O., P. Hacker, N. Maximenko, G. Lagerloef, and J. Potemra, 2016: Optimum interpolation analysis of Aquarius sea surface salinity. *J. Geophys. Res. Oceans*, **121**, 602–616, <https://doi.org/10.1002/2015JC011343>.
- Morison, J., R. Andersen, N. Larson, E. D'Asaro, and T. Boyd, 1994: The correction for thermal-lag effects in Sea-Bird CTD data. *J. Atmos. Oceanic Technol.*, **11**, 1151–1164, [https://doi.org/10.1175/1520-0426\(1994\)011<1151:TCFTLE>2.0.CO;2](https://doi.org/10.1175/1520-0426(1994)011<1151:TCFTLE>2.0.CO;2).
- Mulet, S., and Coauthors, 2021: The new CNES-CLS18 global mean dynamic topography. *Ocean Sci.*, **17**, 789–808, <https://doi.org/10.5194/os-17-789-2021>.
- Murty, V. S. N., Y. V. B. Sarma, D. Panakala Rao, and C. S. Murty, 1992: Water characteristics, mixing and circulation in the Bay of Bengal during southwest monsoon. *J. Mar. Res.*, **50**, 207–228, <https://doi.org/10.1357/002224092784797700>.
- Pirro, A., H. J. S. Fernando, H. W. Wijesekera, T. G. Jensen, L. Centurioni, and S. U. P. Jinadasa, 2020a: Eddies and currents in the Bay of Bengal during summer monsoons. *Deep-Sea Res. II*, **172**, 104728, <https://doi.org/10.1016/j.dsr2.2019.104728>.
- , H. Wijesekera, E. Jarosz, and H. J. S. Fernando, 2020b: Dynamics of intra-seasonal oscillations in Bay of Bengal during summer monsoons captured by mooring observations. *Deep-Sea Res. II*, **172**, 104718, <https://doi.org/10.1016/j.dsr2.2019.104718>.
- Rao, R. R., and R. Sivakumar, 2003: Seasonal variability of sea surface salinity and salt budget of the mixed layer of the north Indian Ocean. *J. Geophys. Res.*, **108**, 3009, <https://doi.org/10.1029/2001JC000907>.
- , M. S. Girishkumar, M. Ravichandran, B. K. Samala and S. Nandakumar, 2006: Observed mini-cold pool off the southern tip of India and its intrusion into the south central Bay of Bengal during summer monsoon season. *Geophys. Res. Lett.*, **33**, L06607, <https://doi.org/10.1029/2005GL025382>.
- , M. S. Girish Kumar, M. Ravichandran, A. R. Rao, V. V. Gopalakrishna, and P. Thadathil, 2010: Interannual variability of kelvin wave propagation in the wave guides of the equatorial Indian Ocean, the coastal Bay of Bengal and the south-eastern Arabian Sea during 1993–2006. *Deep-Sea Res. I*, **57**, 1–13, <https://doi.org/10.1016/j.dsr.2009.10.008>.
- , V. Jitendra, M. S. Girish, M. Kumar, M. Ravichandran, and S. S. V. S. Ramakrishna, 2015: Interannual variability of the Arabian Sea warm pool: Observations and governing mechanisms. *Climate Dyn.*, **44**, 2119–2136, <https://doi.org/10.1007/s00382-014-2243-0>.
- Roman-Stork, H. L., B. Subrahmanyam, and V. S. N. Murty, 2020a: The role of salinity in the southeastern Arabian sea in determining monsoon onset and strength. *J. Geophys. Res. Oceans*, **125**, e2019JC015592, <https://doi.org/10.1029/2019JC015592>.
- , —, and C. B. Trott, 2020b: Monitoring intraseasonal oscillations in the Indian Ocean using satellite observations. *J. Geophys. Res. Oceans*, **125**, e2019JC015891, <https://doi.org/10.1029/2019JC015891>.
- Sanchez-Franks, A., B. G. M. Webber, B. A. King, P. N. Vinayachandran, A. J. Matthews, P. M. F. Sheehan, A. Behara, and C. P. Neema, 2019: The railroad switch effect of seasonally reversing currents in the Bay of Bengal high-salinity core. *Geophys. Res. Lett.*, **46**, 6005–6014, <https://doi.org/10.1029/2019GL082208>.
- Schauer, U., and M. Losch, 2019: “Freshwater” in the ocean is not a useful parameter in climate research. *J. Phys. Oceanogr.*, **49**, 2309–2321, <https://doi.org/10.1175/JPO-D-19-0102.1>.
- Schott, F. A., and J. P. McCreary Jr., 2001: The monsoon circulation of the Indian Ocean. *Prog. Oceanogr.*, **51**, 1–123, [https://doi.org/10.1016/S0079-6611\(01\)00083-0](https://doi.org/10.1016/S0079-6611(01)00083-0).
- , J. Reppin, J. Fischer, and D. Quadfasel, 1994: Currents and transports of the monsoon current south of Sri Lanka. *J. Geophys. Res.*, **99**, 25 127–25 141, <https://doi.org/10.1029/94JC02216>.
- Shankar, D., P. N. Vinayachandran, and A. S. Unnikrishnan, 2002: The monsoon currents in the north Indian Ocean. *Prog. Oceanogr.*, **52**, 63–120, [https://doi.org/10.1016/S0079-6611\(02\)00024-1](https://doi.org/10.1016/S0079-6611(02)00024-1).
- Shroyer, E., and Coauthors, 2021: Bay of Bengal intraseasonal oscillations and the 2018 monsoon onset. *Bull. Amer. Meteor. Soc.*, **102**, E1936–E1951, <https://doi.org/10.1175/BAMS-D-20-0113.1>.
- Su, D., S. Wijeratne, and C. B. Pattiaratchi, 2021: Monsoon influence on the island mass effect around the Maldives and Sri Lanka. *Front. Mar. Sci.*, **8**, 645672, <https://doi.org/10.3389/fmars.2021.645672>.
- Talley, L. D., 2008: Freshwater transport estimates and the global overturning circulation: Shallow, deep and throughflow components. *Prog. Oceanogr.*, **78**, 257–303, <https://doi.org/10.1016/j.pocan.2008.05.001>.

- Todd, R. E., 2020: Equatorial circulation in the western Indian Ocean during onset of the 2018 summer monsoon and links to the Bay of Bengal. *Geophys. Res. Lett.*, **47**, e2020GL087215, <https://doi.org/10.1029/2020GL087215>.
- Vinayachandran, P. N., and T. Yamagata, 1998: Monsoon response of the sea around Sri Lanka: Generation of thermal domes and anticyclonic vortices. *J. Phys. Oceanogr.*, **28**, 1946–1960, [https://doi.org/10.1175/1520-0485\(1998\)028<1946:MR0TSA>2.0.CO;2](https://doi.org/10.1175/1520-0485(1998)028<1946:MR0TSA>2.0.CO;2).
- , Y. Masumoto, T. Mikawa, and T. Yamagata, 1999: Intrusion of the southwest monsoon current into the Bay of Bengal. *J. Geophys. Res.*, **104**, 11 077–11 085, <https://doi.org/10.1029/1999JC900035>.
- , V. S. N. Murty, and V. Ramesh Babu, 2002: Observations of barrier layer formation in the Bay of Bengal during summer monsoon. *J. Geophys. Res.*, **107**, 8018, <https://doi.org/10.1029/2001JC000831>.
- , P. Chauhan, M. Mohan, and S. Nayak, 2004: Biological response of the sea around Sri Lanka to summer monsoon. *Geophys. Res. Lett.* **31**, L01302, <https://doi.org/10.1029/2003GL018533>.
- , T. Kagimoto, Y. Masumoto, P. Chauhan, S. R. Nayak, and T. Yamagata, 2005: Bifurcation of the east India coastal current east of Sri Lanka. *Geophys. Res. Lett.*, **32**, L15606, <https://doi.org/10.1029/2005GL022864>.
- , C. P. Neema, S. Mathew, and R. Remya, 2012: Mechanisms of summer intraseasonal sea surface temperature oscillations in the Bay of Bengal. *J. Geophys. Res.*, **117**, C01005, <https://doi.org/10.1029/2011JC007433>.
- , D. Shankar, S. Vernekar, K. K. Sandeep, P. Amol, C. P. Neema, and A. Chatterjee, 2013: A summer monsoon pump to keep the Bay of Bengal salty. *Geophys. Res. Lett.*, **40**, 1777–1782, <https://doi.org/10.1002/grl.50274>.
- , and Coauthors, 2018: BoBBLE (Bay of Bengal Boundary Layer Experiment): Ocean–atmosphere interaction and its impact on the south Asian monsoon. *Bull. Amer. Meteor. Soc.*, **99**, 1569–1587, <https://doi.org/10.1175/BAMS-D-16-0230.1>.
- Webber, B. G. M., A. J. Matthews, P. N. Vinayachandran, C. P. Neema, A. Sanchez-Franks, V. Vijith, P. Amol, and D. B. Baranowski, 2018: The dynamics of the southwest monsoon current in 2016 from high-resolution in situ observations and models. *J. Phys. Oceanogr.*, **48**, 2259–2282, <https://doi.org/10.1175/JPO-D-17-0215.1>.
- Wentz, F. J., C. Gentemann, D. Smith, and D. Chelton, 2000: Satellite measurements of sea surface temperature through clouds. *Science*, **288**, 847–850, <https://doi.org/10.1126/science.288.5467.847>.
- Wijesekera, H. W., and Coauthors, 2015: Southern Bay of Bengal currents and salinity intrusions during the northeast monsoon. *J. Geophys. Res. Oceans*, **120**, 6897–6913, <https://doi.org/10.1002/2015JC010744>.
- , W. J. Teague, D. W. Wang, E. Jaroz, T. G. Jensen, S. U. P. Jinadasa, H. J. S. Fernando, and Z. R. Hallock, 2016a: Low frequency currents from deep moorings in the southern Bay of Bengal. *J. Phys. Oceanogr.*, **46**, 3209–3238, <https://doi.org/10.1175/JPO-D-16-0113.1>.
- , and Coauthors, 2016b: ASIRI: An ocean–atmosphere initiative for Bay of Bengal. *Bull. Amer. Meteor. Soc.*, **97**, 1859–1884, <https://doi.org/10.1175/BAMS-D-14-00197.1>.